

CKAA: Cross-subspace Knowledge Alignment and Aggregation for Robust Continual Learning

Lingfeng He, De Cheng, Zhiheng Ma, Huaijie Wang, Dingwen Zhang, Nannan Wang, *Senior Member, IEEE*, Xinbo Gao, *Fellow, IEEE*

Abstract—Continual Learning (CL) empowers AI models to continuously learn from sequential task streams. Recently, parameter-efficient fine-tuning (PEFT)-based CL methods have garnered increasing attention due to their superior performance. They typically allocate a unique sub-module for learning each task, with a task recognizer to select the appropriate sub-modules for testing images. However, due to the feature subspace misalignment from independently trained sub-modules, these methods tend to produce ambiguous decisions under misleading task-ids. To address this, we propose Cross-subspace Knowledge Alignment and Aggregation (CKAA), a novel framework that enhances model robustness against misleading task-ids through two key innovations: (1) Dual-level Knowledge Alignment (DKA): By aligning intra-class feature distributions across different subspaces and learning a robust global classifier through a feature simulation process, DKA enables the model to distinguish features from both correct and incorrect subspaces during training. (2) Task-Confidence-guided Mixture of Adapters (TC-MoA): A robust inference scheme that adaptively aggregates task-specific knowledge from relevant sub-modules based on task-confidence scores, avoiding overconfidence in misleading task-id predictions. Extensive experiments demonstrate that CKAA outperforms existing PEFT-based CL methods.

Index Terms—Continual learning, parameter-efficient, cross-subspace, knowledge alignment

I. INTRODUCTION

Continual Learning (CL) requires the model to continuously learn from sequentially arriving data streams, which is essential for AI models to adapt to the ever-evolving real-world scenarios [1]–[3]. CL presents a major challenge: as the model is updated to accommodate new categories, they often suffer from catastrophic forgetting [4]–[7], wherein knowledge of old classes is diminished. There are two common scenarios in CL: Task-Incremental Learning (TIL) [8] and Class-Incremental Learning (CIL) [9]. We investigate the more challenging CIL setting with unknown task-ids during inference [10], [11].

This work was supported in part by the National Natural Science Foundation of China (NSFC) under Grant 62176198 and U22A2096; in part by the Key R&D Program of Shaanxi Province under Grant 2024GX-YBXM-135, in part by the Key Laboratory of Big Data Intelligent Computing under Grant BDIC-2023-A-004.

Lingfeng He, De Cheng and Nannan Wang are with School of Telecommunications Engineering, Xidian University, Xi'an, China (email: lfhe@stu.xidian.edu.cn, dcheng@xidian.edu.cn, nnwang@xidian.edu.cn). Huaijie Wang, Xinbo Gao are with School of Electronic Engineering, Xidian University, Xi'an, China (email: huaijie_wang@stu.xidian.edu.cn, xbgao@mail.xidian.edu.cn). Zhiheng Ma is with SUAT-Faculty of Computational Microelectronics, Shenzhen University of Advanced Technology, Shenzhen, China (email: mazhiheng@suat-sz.edu.cn). Dingwen Zhang is with the Brain and Artificial Intelligence Laboratory, Northwestern Polytechnical University, Xi'an, China (email: zdw2006yyy@nwpu.edu.cn).

Corresponding Author: De Cheng

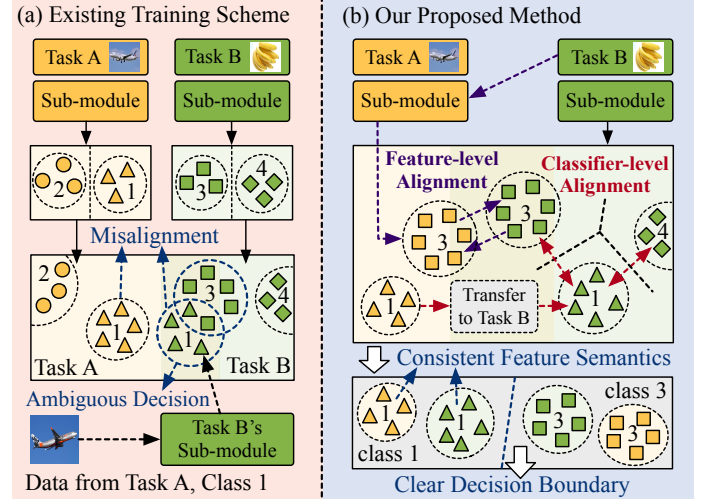


Fig. 1. Illustration of our motivation. Existing methods (a) encounter ambiguous decisions for features projected into the incorrect subspace due to the misalignment between subspaces. Our CKAA (b) addresses this by semantically aligning feature distributions across subspaces and learning robust decision boundaries, effectively distinguishing wrongly projected features.

With the advancement of pre-trained models, Parameter Efficient Fine-Tuning (PEFT)-based methods [12]–[15] exhibit superior performance in vision tasks. These methods keep the pre-trained backbone frozen while inserting lightweight modules for training. PEFT-based methods have been investigated in the field of CL [16]–[18] and have proven highly effective in mitigating catastrophic forgetting by maintaining the strong generalizability of pre-trained models throughout sequential training.

Several methods [16], [19]–[21] are proposed to harness the potential of PEFT methods in the field of CIL. They typically allocate a dedicated sub-module for each task, effectively uncovering the unique knowledge for each task and ensuring model plasticity for new tasks. Since task-ids are unavailable during CIL inference, a task recognizer is designed to identify task-ids and select the appropriate sub-module for testing images. Unfortunately, task-id misidentification is inevitable, leading to features being erroneously projected into incorrect subspaces, which in turn results in ambiguous and unreliable decisions. As illustrated in Fig.1(a), when an image from [Task A, Class 1] selects an improper [sub-module B], the model delivers an ambiguous decision between Class 1 and Class 3 for the feature within task B's subspace, resulting in prediction errors. Such errors stem from the misaligned feature subspaces caused by the independent training and diverse optimization objectives of the sub-modules, where the classifier fails to distinguish wrongly projected features

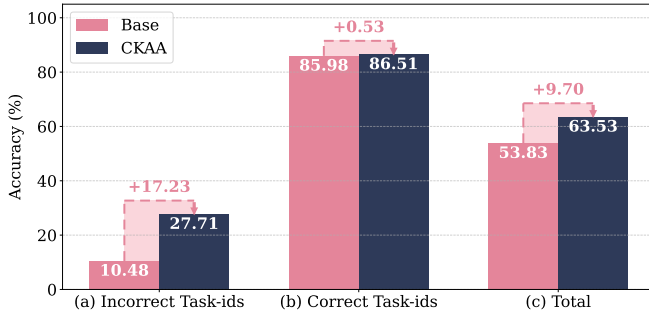


Fig. 2. Classification accuracy of samples with correct and incorrect task-ids.

within incorrect subspaces, despite their meaningful semantic information.

As shown in Fig.2, we visualize the classification accuracy of samples predicted with (a) correct and (b) incorrect task-ids on 10S-ImageNetA. The term **Base** refers to performance obtained using task-specific modules trained independently. It suffers from the misalignment problem, resulting in poor accuracy (10.48%). These observations highlight the vulnerability of the model’s robustness when provided with incorrect task-ids, leading to performance degradation. We further consider that the misalignment issue is mainly reflected in two aspects: (1) The feature semantics of the same image from the correct and incorrect sub-modules remain inconsistent; (2) The decision boundaries trained solely with correct task-ids cannot classify features within incorrect subspaces.

Motivated by these analysis, we propose a novel Cross-subspace Knowledge Alignment and Aggregation (CKA) framework, including a knowledge alignment training approach and a knowledge aggregation inference scheme, effectively mitigating the misalignment issue. We build a visual prompt-based task recognizer, alongside dedicated task-specific sub-modules to maintain model plasticity. For training these sub-modules, we propose a Dual-level Knowledge Alignment (DKA, Fig.1(b)) approach that aligns feature semantics and decision boundaries across different subspaces. Our feature-level alignment groups the same class features from different tasks’ subspaces together, aligning intra-class feature distributions in all subspaces while enhancing inter-class discriminability. Building upon these semantically unified feature subspaces, we further train a robust global classifier capable of distinguishing features projected into both correct and incorrect subspaces, ensuring reliable prediction even under misleading task-ids. Specifically, we train a task-adaptive classifier for each task to distinguish features of all seen classes projected into its subspace via a feature simulation process. These classifiers are aggregated into a global classifier for robust inference. Consequently, DKA mitigates the misalignment in both two aforementioned aspects.

To further enhance model robustness against misleading task-ids during inference, we propose a Task-Confidence-guided Mixture of Adapters (TC-MoA) scheme, which dynamically aggregates task-specific knowledge from semantically unified sub-modules. Specifically, the task recognizer computes task-confidence scores for each test image, reflecting its semantic relevance to each task. These scores serve as routing weights to adaptively combine intermediate features from task-

specific sub-modules, forming a Mixture of Adapters (MoA) architecture. Unlike existing selection strategies [16], [20], our soft aggregation mechanism avoids overconfidence in misleading task-ids by adaptively integrating knowledge from potentially relevant sub-modules, resulting in a more effective and robust inference framework for CIL frameworks with task-specific design.

The main contributions can be summarized as follows:

- To enhance the model’s robustness against misleading task-ids, we propose a novel CKA framework, which introduces Dual-level Knowledge Alignment (DKA) to align feature semantics and learn robust global decision boundaries across task-specific subspaces, effectively mitigating the misalignment issue.
- A Task-Confidence-guided Mixture of Adapters (TC-MoA) scheme is designed to adaptively aggregate knowledge from potentially relevant sub-modules during inference, avoiding overconfidence in misleading task-ids.
- Extensive experiments on four mainstream CL benchmarks demonstrate that the proposed CKA outperforms existing state-of-the-art methods.

II. RELATED WORKS

A. Continual Learning

Continual Learning aims to update the model with new data while mitigating catastrophic forgetting [6], [7], [22] of previously acquired knowledge. Traditional methods can be categorized into replay-based [23]–[26], regularization-based [27]–[30], and expansion-based methods [31]–[34]. Replay-based methods maintain a memory buffer to store the instances of previous tasks. Regularization-based methods introduce penalty terms to prevent substantial changes in the parameters important for old tasks. Expansion-based methods freeze specific parameters for old tasks while allocating new parameters for subsequent tasks.

Recently, continual learning with pre-trained models [16], [19], [20], [35]–[38] have gained growing attention, owing to the strong representation capacity of pre-trained models. Some methods fully fine-tune the pre-trained models [39], [40], which is highly time-consuming. Other methods incorporate PEFT methods into continual learning. Prompt pool-based methods [16], [19], [20], [41] maintain a prompt pool for all tasks and select appropriate prompts for each specific task. Some adapter-based methods [17], [18], [21] build expandable adapter-based architecture while reducing catastrophic forgetting through regularization terms or semantic adjustment. PGP [42] and VPT-NSP [3] integrate orthogonal projection into the prompt-based methods, achieving impressive performance and establishing a simple-yet-effective baseline for PEFT-based continual learning.

B. Parameter-Efficient Fine-Tuning

Parameter-Efficient Fine-Tuning (PEFT) is a paradigm to fine-tune pre-trained models by inserting sub-modules with a small number of parameters while keeping the pre-trained parameters frozen. PEFT methods have shown superior performance in NLP [12], [43], [44]. Recently, PEFT methods

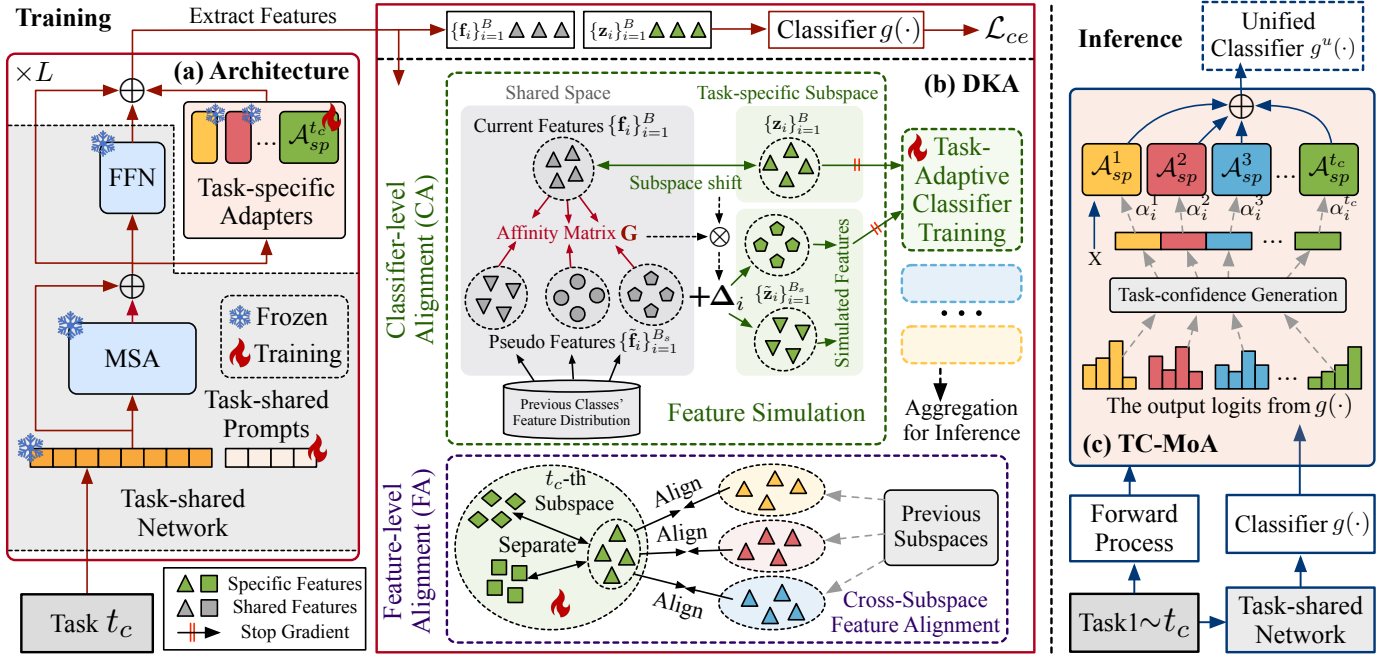


Fig. 3. The framework of our proposed method. Our network architecture (a) is composed of a visual prompt-based task-shared network and adapter-based task-specific sub-modules. To enhance the model's robustness against incorrect task-ids, we propose Dual-level Knowledge Alignment approach (b, DKA), which aligns task-specific knowledge at the feature and classifier levels. During inference, the Task-Confidence-guided Mixture of Adapters (c, TC-MoA) effectively aggregates task-specific knowledge into the task-shared backbone.

have been proposed for Vision Transformer (ViT) [45]–[47]. Prompt Tuning [14], [48], [49] and Prefix-Tuning [44] prepend a set of learnable tokens to the inputs before the transformer blocks. Adapter [13] inserts lightweight modules into the Feed Forward Network (FFN) and Low-Rank Adaptation (LoRA) [12] injects learnable rank decomposition matrices to re-parameterize the pre-trained weights. Mixture-of-Experts (MoE) [50] aggregates multiple sub-networks as experts via a routing network. The above PEFT methods have demonstrated comparable performance to full fine-tuning.

III. METHODOLOGY

Problem Definition. In Continual Learning, there is a sequence of tasks with non-overlapping classes. We define the sequential dataset as $\mathcal{D} = \{\mathcal{D}_1, \dots, \mathcal{D}_T\}$. $\mathcal{D}_t = \{\mathbf{x}_i^t, y(\mathbf{x}_i^t)\}_{i=1}^{|\mathcal{D}_t|}$ is the dataset associated with the t -th task of size $|\mathcal{D}_t|$, and $y(\mathbf{x}_i^t) \in \mathcal{Y}^t$ denotes the corresponding class of $\mathbf{x}_i^t \in \mathbb{R}^{H \times W \times C}$. \mathcal{Y}^t is the label space of task t , and $\mathcal{Y}^t \cap \mathcal{Y}^{t'} = \emptyset$ for $t \neq t'$. The objective of continual learning is to train a model sequentially on T tasks and perform well on testing images from all seen classes $\mathcal{Y}^1 \cup \dots \cup \mathcal{Y}^T$.

We follow existing PEFT-based methods [16], [17], [19] and assume that a pre-trained Vision Transformer (ViT) [51] is available for model initialization. The model is decoupled into a feature extractor $\mathcal{F} : \mathbb{R}^{H \times W \times C} \rightarrow \mathbb{R}^d$ and a classifier $g : \mathbb{R}^d \rightarrow \mathbb{R}^{\sum_{t=1}^T |\mathcal{Y}^t|}$. Similar to existing work [16], we focus on the Class-Incremental Learning (CIL) setting, where task-ids are unknown during inference.

Overall Framework. The overall framework of our CKAA is illustrated in Fig.3. Our network architecture (Fig.3(a)) consists of a task-shared network to function as a task recognizer, and task-specific sub-modules to capture unique knowledge for individual tasks. To enhance the model's robustness

against incorrect task-ids, we propose a Dual-level Knowledge Alignment (DKA, Fig.3(b)) approach for training these sub-modules. Our DKA consists of two components: (1) Feature-level Alignment (FA), which groups the same class features from different feature subspaces together; (2) Classifier-level Alignment (CA), which learns a task-adaptive classifier during each session to address cases where previous images are incorrectly assigned with the current task-id, and aggregates them to build a robust global classifier for inference. During inference, we introduce a Task-Confidence-guided Mixture of Adapters (TC-MoA, Fig.3(c)) approach, which generates task-confidence scores as routing weights to adaptively aggregate task-specific knowledge without task-ids.

A. Network Architecture

Our network architecture is composed of: (1) A trainable task-shared network, which serves as a task recognizer and captures the common knowledge from the downstream task; (2) Task-specific sub-modules, which explore the unique knowledge for individual tasks and ensure model plasticity.

Task-shared Network. We develop our task-shared component on top of Visual Prompt Tuning (VPT) [45]. Since the visual prompts can inject knowledge before each transformer block as a global operation, they are well-suited to capturing the common knowledge of downstream tasks with strong generalizability. Specifically, a set of task-shared learnable vectors denoted as $\mathcal{P}_{sh} = \{\mathbf{P}_l\}_{l=1}^L$, are inserted into the original input at each transformer block, where $\mathbf{P}_l \in \mathbb{R}^{N_p \times d}$ is the prompt corresponding to the l -th block. At l -th block, the prompt \mathbf{P}_l is concatenated with the patch representations \mathbf{X}_l to serve as the input to the MSA layer:

$$[\hat{\mathbf{X}}_l, \hat{\mathbf{P}}_l] = \text{MSA}([\mathbf{X}_l; \mathbf{P}_l]); \quad \mathbf{X}_{l+1} = \text{FFN}(\hat{\mathbf{X}}_l), \quad (1)$$

where $\text{MSA}(\cdot)$ and $\text{FFN}(\cdot)$ denotes the Multi-head Self-Attention (MSA) layer and the Feed Forward Network (FFN) layer in ViT. The pre-trained feature extractor \mathcal{F} and the prompts \mathcal{P}_{sh} work together to serve as the task-shared network, the shared feature representation of input \mathbf{x} is denoted as $\mathbf{f} = \mathcal{F}(\mathbf{x}; \mathcal{P}_{sh})$. Since the task-shared network should adapt to all downstream tasks, it is essential to mitigate its forgetting when training new tasks. To achieve this objective, we update \mathcal{P}_{sh} orthogonally to the previous feature space following [3], [42], [52]. These prompts \mathcal{P}_{sh} are updated throughout all sequential tasks, encapsulating the common knowledge among them. Such orthogonally optimized prompts establish a shared backbone and a powerful task recognizer, tailored for downstream tasks.

Task-specific Sub-modules. Due to the stringent orthogonal constraints, the task-shared network is insufficient to capture fine-grained knowledge specific to each individual task, thereby limiting the model's plasticity. Therefore, we allocate a task-specific sub-module for each task to capture its unique knowledge and generate more discriminative features. We design task-specific sub-modules based on an adapter architecture [13], denoted as $\mathcal{A}_{sp}^t = \{\mathcal{A}_l^t\}_{l=1}^L$. Since the residual connection nature of adapter-tuning, it can effectively enable the model to aggregate unique knowledge from different tasks independently. For the adapter $\mathcal{A}_l^t \in \mathcal{A}_{sp}^t$ in l -th block, it is composed of a downsampling matrix $\mathbf{W}_{down} \in \mathbb{R}^{d \times \hat{d}}$ and an upsampled matrix $\mathbf{W}_{up} \in \mathbb{R}^{\hat{d} \times d}$. Denote the input as \mathbf{X} , the forward process can be formulated as $\mathcal{A}(\mathbf{X}) = \text{ReLU}(\mathbf{X} \cdot \mathbf{W}_{down}) \cdot \mathbf{W}_{up}$. At l -th block, \mathcal{A}_l^t incorporate task-specific knowledge in the FFN layer through a residual connection:

$$\mathbf{X}_{l+1} = \text{FFN}(\hat{\mathbf{X}}_l) + \mathcal{A}_l^t(\hat{\mathbf{X}}_l). \quad (2)$$

The final task-specific feature of input \mathbf{x} is denoted as $\mathbf{z} = \mathcal{F}(\mathbf{x}; \mathcal{P}_{sh}, \mathcal{A}_{sp}^t)$.

Basic loss. During t_c -th session, given a batch $\{\mathbf{x}_i\}_{i=1}^B$ of size B (with the superscript t_c omitted for simplicity), the features $\{\mathbf{f}_i\}_{i=1}^B$ and $\{\mathbf{z}_i\}_{i=1}^B$ from the shared network and the t_c -th sub-module are extracted, where $\mathbf{f}_i = \mathcal{F}(\mathbf{x}_i; \mathcal{P}_{sh})$ and $\mathbf{z}_i = \mathcal{F}(\mathbf{x}_i; \mathcal{P}_{sh}, \mathcal{A}_{sp}^t)$. These features are trained with the classifier g and a commonly-used cross-entropy loss:

$$\mathcal{L}_{ce} = \frac{1}{B} \sum_{i=1}^B \mathcal{L}(\sigma(g(\mathbf{f}_i)), y(\mathbf{f}_i)) + \mathcal{L}(\sigma(g(\mathbf{z}_i)), y(\mathbf{z}_i)), \quad (3)$$

where $y(\mathbf{f})$ represents the ground-truth class label of feature \mathbf{f} . \mathcal{L} denotes the standard cross-entropy loss, and $\sigma(\cdot)$ denotes the softmax operation. Following existing methods [3], [16], [20], g is trained separately on the classes of each task, and the weights are concatenated for inference.

B. Dual-level Knowledge Alignment

Given the design of our task-specific sub-modules, it is essential to select appropriate sub-modules by estimating task-ids through the task recognizer during inference. However, there are always inevitable incorrect task-ids predictions. To enhance the model's robustness against these incorrect task-ids, we propose a Dual-level Knowledge Alignment (DKA)

training approach, which enhances subspace alignment at the feature and classifier levels.

Feature-level Alignment (FA). For a robust feature extractor capable of generating meaningful features despite incorrect task-ids, the same image should achieve consistent semantics when projected into the correct and the incorrect feature subspaces. Therefore, we semantically unify features across different feature subspaces through FA. Specifically, we propose a Cross-Subspace Feature Alignment (CSFA) loss, which encourages features of the same class in the current subspace to align with those in the previous subspace. We first extract the features of the current dataset \mathcal{D}_{t_c} in the t_p -th previous subspace for $t_p < t_c$, denoted as $\tilde{\mathbf{z}}_i^{t_c \rightarrow t_p} = \mathcal{F}(\mathbf{x}_i^{t_c}; \mathcal{P}_{sh}, \mathcal{A}_{sp}^{t_p})$ and $\tilde{\mathbf{x}}_i^{t_c} \in \mathcal{D}_{t_c}$. During training, we randomly sample a feature set $\tilde{\mathcal{C}}_{sp} = \{\tilde{\mathbf{z}}_j^{t_c \rightarrow t_p}\}_{j=1}^B$ in previous subspaces. Given an input batch $\mathcal{C}_{sp} = \{\mathbf{z}_i\}_{i=1}^B$, for a feature $\mathbf{z}_k \in \mathcal{C}_{sp}$ with label $y(\mathbf{z}_k)$ in the current subspace, we build its positive set by features from the sampled set with the same ground-truth, where $\mathcal{P}(\mathbf{z}_k) = \{\tilde{\mathbf{z}}_j^{t_c \rightarrow t_p} | y(\tilde{\mathbf{z}}_j^{t_c \rightarrow t_p}) = y(\mathbf{z}_k), \tilde{\mathbf{z}}_j^{t_c \rightarrow t_p} \in \tilde{\mathcal{C}}_{sp}\}$. Meanwhile, the features from the current subspace with different labels are regarded as the negative samples, where $\mathcal{N}(\mathbf{z}_k) = \{\mathbf{z}_j | y(\mathbf{z}_j) \neq y(\mathbf{z}_k), \mathbf{z}_j \in \mathcal{C}_{sp}\}$. Then CSFA loss for an input batch $\{\mathbf{z}_i\}_{i=1}^B$ is formulated as follows:

$$\mathcal{L}_{csfa} = -\frac{1}{B} \sum_{i=1}^B \log \frac{\sum_{\mathbf{z}^+ \in \mathcal{P}(\mathbf{z}_i)} \exp(\text{sim}(\mathbf{z}_i, \mathbf{z}^+)/\tau_f)}{\sum_{\mathbf{z}_j \in \mathcal{P}(\mathbf{z}_i) \cup \mathcal{N}(\mathbf{z}_i)} \exp(\text{sim}(\mathbf{z}_i, \mathbf{z}_j)/\tau_f)}, \quad (4)$$

where τ_f is a temperature factor for contrastive learning. The CSFA loss groups the same class features together in different subspaces, alleviating feature-level misalignment.

Classifier-level Alignment (CA). Building upon the semantically unified subspaces enhanced by FA, CA aims to train a robust global classifier capable of distinguishing features across all subspaces even under incorrect task-ids. Specifically, in t_c -th session, we train a task-adaptive classifier g^{t_c} , which seeks to avoid ambiguous predictions when previous data $\mathbf{x}_i^{t_c} \in \mathcal{D}_1 \cup \dots \cup \mathcal{D}_{t_c-1}$ are projected into the current feature subspace. To achieve this objective, we first simulate the features of the previous data in the current subspace, then the simulated features are used to jointly train g^{t_c} alongside the current features. We further decompose the simulation process into *three steps*: (1) **Modeling the affinities** between current and previous data within the shared feature space through the task-shared network; (2) **Modeling the subspace shift** within current data between the current subspace and the shared ones; (3) **Transferring the subspace shift** of the current shared features to the previous ones through the affinity matrix.

Since modeling the affinities requires the previous data distributions but there are no exemplars saved for training, we address this issue through Gaussian sampling. After the t -th session, for the k -th class in the t -th task, we approximate its feature distribution in the shared feature space as a Gaussian distribution $\mathcal{G}_{k,t}$. During the t_c -th session, for each arriving batch, we sample pseudo representations $\mathcal{S}_{sh} = \{\tilde{\mathbf{f}}_i, y(\tilde{\mathbf{f}}_i)\}_{i=1}^{B_s}$ with size B_s from previous shared feature distributions $\cup_{t \leq t_c-1} \mathcal{G}_{k,t}$. In conjunction with the current features $\mathcal{C}_{sh} = \{\mathbf{f}_i, y(\mathbf{f}_i)\}_{i=1}^B$ and $\mathcal{C}_{sp} = \{\mathbf{z}_i, y(\mathbf{z}_i)\}_{i=1}^B$, the affinity matrix $\mathbf{G} \in \mathbb{R}^{B_s \times B}$ between the previous data and

current data in the shared feature space are formulated as follows:

$$\mathbf{G}_{ij} = \begin{cases} \exp(\text{sim}(\tilde{\mathbf{f}}_i, \mathbf{f}_j)/\tau_g), & \text{if } \mathbf{f}_j \in \mathcal{K}(\tilde{\mathbf{f}}_i, K_g), \\ 0, & \text{otherwise,} \end{cases} \quad (5)$$

where τ_g is a temperature factor. $\text{sim}(\mathbf{a}, \mathbf{b})$ denotes the cosine similarity between vector \mathbf{a} and \mathbf{b} , where $\text{sim}(\mathbf{a}, \mathbf{b}) = \mathbf{a}^\top \mathbf{b} / (\|\mathbf{a}\| \cdot \|\mathbf{b}\|)$. $\mathcal{K}(\tilde{\mathbf{f}}_i, K_g)$ denotes the K_g nearest neighbors in \mathcal{C}_{sh} of $\tilde{\mathbf{f}}_i$. \mathbf{G}_{ij} represents the affinity between sampled feature $\tilde{\mathbf{f}}_i$ and current feature \mathbf{f}_j .

The subspace shift of current data between the current subspace and the shared feature space can be simply modeled by the residual between the specific feature $\{\mathbf{z}_i\}_{i=1}^B$ and the shared feature $\{\mathbf{f}_i\}_{i=1}^B$ of current data. Subsequently, we transfer the subspace shift from the current features $\{\mathbf{f}_i\}_{i=1}^B$ to the sampled pseudo features $\{\tilde{\mathbf{f}}_i\}_{i=1}^B$. The simulated features $\{\tilde{\mathbf{z}}_i\}_{i=1}^B$ are derived as follows:

$$\tilde{\mathbf{z}}_i = \tilde{\mathbf{f}}_i + \Delta_i, \quad \Delta_i = \frac{\sum_{j=1}^B \mathbf{G}_{ij}(\mathbf{z}_j - \mathbf{f}_j)}{\sum_{j=1}^B \mathbf{G}_{ij}}. \quad (6)$$

Through the above process, we derive the simulated feature set $\mathcal{S}_{sp} = \{\tilde{\mathbf{z}}_i, y(\tilde{\mathbf{z}}_i)\}_{i=1}^B$. Then we obtain the unified feature set $\mathcal{U} = \mathcal{S}_{sh} \cup \mathcal{S}_{sp} \cup \mathcal{C}_{sh} \cup \mathcal{C}_{sp}$, which includes features of images from all seen tasks in the current subspace. We utilize it to train the task-adaptive classifier g^{t_c} :

$$\mathcal{L}_{ca} = \frac{1}{|\mathcal{U}|} \sum_{\{\mathbf{f}, y(\mathbf{f})\} \in \mathcal{U}} \mathcal{L}(\sigma(g^{t_c}(\mathbf{f})), y(\mathbf{f})). \quad (7)$$

After training t_c -th session, to reduce computational overhead for inference, we aggregate the parameters from all the task-adaptive classifiers, *i.e.*, g^1, \dots, g^{t_c} , to build a global classifier g^u that fits all the task-specific feature subspaces. For the parameter corresponding to the k -th class in the t_p -th task, *i.e.*, $k \in \mathcal{Y}^{t_p}$, the parameter aggregation can be formulated as follows:

$$\mathbf{W}^u[k] = \frac{\sum_{t=t_p}^{t_c} \mathbf{W}^t[k]}{t_c - t_p + 1}, \quad \mathbf{b}^u[k] = \frac{\sum_{t=t_p}^{t_c} \mathbf{b}^t[k]}{t_c - t_p + 1}, \quad (8)$$

where $\mathbf{W}^u[k]$ ($\mathbf{b}^u[k]$) is the k -th class's weight (bias) in g^u , and $\mathbf{W}^t[k]$ ($\mathbf{b}^t[k]$) is the k -th class's weight (bias) in g^t . Such an aggregation strategy enables the global classifier to differentiate features projected into all subspaces, even when confronted with misleading task-ids.

C. Optimization

The overall framework is trained by minimizing:

$$\mathcal{L} = \mathcal{L}_{ce} + \mathcal{L}_{csfa} + \mathcal{L}_{ca}. \quad (9)$$

For simplicity, the trade-off parameters for all loss terms are set to 1.0. During each training session, our framework can be optimized in an end-to-end fashion. The overall training pipeline is outlined in Alg.1.

Algorithm 1 Training pipeline for task t_c

Inputs: Dataset \mathcal{D}_{t_c} , backbone \mathcal{F} , shared prompts \mathcal{P}_{sh} , adapter $\mathcal{A}_{sp}^{t_c}$.
Outputs: Updated \mathcal{P}_{sh} , $\mathcal{A}_{sp}^{t_c}$, classifier g^{t_c} .

- 1: Initialize $\mathcal{A}_{sp}^{t_c}$ and g^{t_c} ; **if** $t_c = 1$, initialize \mathcal{P}_{sh} ;
- 2: **for** $\{\mathbf{x}_i, y_i\} \in \mathcal{D}_{t_c}$ **do**
- 3: $\mathbf{f}_i = \mathcal{F}(\mathbf{x}_i; \mathcal{P}_{sh})$; // Shared features
- 4: $\mathbf{z}_i = \mathcal{F}(\mathbf{x}_i; \mathcal{P}_{sh}, \mathcal{A}_{sp}^{t_c})$; // Specific features
- 5: Compute \mathcal{L}_{ce} (Eq.3);
- 6: **if** $t_c > 1$ **then**
- 7: Extract $\tilde{\mathbf{z}}_i^{t_c \rightarrow t_p} = \mathcal{F}(\mathbf{x}_i; \mathcal{P}_{sh}, \mathcal{A}_{sp}^{t_p})$;
- 8: Compute \mathcal{L}_{csfa} (Eq.4); // Feature-level alignment
- 9: Sample \mathcal{S}_{sh} from $\cup_{t < t_c} \mathcal{G}_{k,t}$;
- 10: Compute affinities \mathbf{G} (Eq.5);
- 11: Simulate \mathcal{S}_{sp} (Eq.6);
- 12: Compute \mathcal{L}_{cu} (Eq.7); // Classifier-level alignment
- 13: **end if**
- 14: Compute total loss \mathcal{L} (Eq.9);
- 15: Update \mathcal{P}_{sh} , $\mathcal{A}_{sp}^{t_c}$, g^{t_c} ;
- 16: **end for**
- 17: **for** class $y \in \mathcal{Y}^{t_c}$ **do**
- 18: Compute \mathcal{G}_{y,t_c} via feature statistics;
- 19: **end for**
- 20: Build unified classifier g^u (Eq.8);

Algorithm 2 Inference pipeline after task t_c

Inputs: Test dataset $\{\mathbf{x}_i\}_{i=1}^N$, backbone \mathcal{F} , prompts \mathcal{P}_{sh} , adapters $\{\mathcal{A}_{sp}^t\}_{t=1}^{t_c}$, unified classifier g^u .
Outputs: Predictions $\{\hat{k}_i\}_{i=1}^N$.

- 1: **for** \mathbf{x}_i in $\{\mathbf{x}_i\}_{i=1}^N$ **do**
- 2: $\mathbf{f}_i = \mathcal{F}(\mathbf{x}_i; \mathcal{P}_{sh})$; // Shared features
- 3: Compute task-confidence $\{P_t(t|\mathbf{f}_i)\}_{t=1}^{t_c}$ (Eq.10, 11);
- 4: $\hat{\mathbf{z}}_i = \mathcal{F}(\mathbf{x}_i; \mathcal{P}_{sh}, \{\mathcal{A}_{sp}^t\}, \{\alpha_i^t\})$; // TC-MoA aggregation
- 5: Predict label \hat{k}_i via g^u and g (Eq.13);
- 6: **end for**

D. Task-Confidence-guided Mixture of Adapters

Given the task-specific nature of our architecture, it is essential to aggregate the task-specific knowledge from relevant sub-modules during inference without task-ids. To achieve this objective, we leverage the task-shared knowledge from the task recognizer to perform an instance-adaptive aggregation for each testing image. Given an image \mathbf{x}_i and its shared feature \mathbf{f}_i , we denote the output of the classifier g before softmax as $g(\mathbf{f}_i) \in \mathbb{R}^K$, and its k -th element as $g(\mathbf{f}_i)[k]$. $K = \sum_{t=1}^{t_c} |\mathcal{Y}^t|$ is the total number of seen classes and t_c is the current task identity. To extract relevant information from each task, we only retain the classes that are semantically related to the testing image, while discarding others. Therefore, we only keep the largest K_c elements in $g(\mathbf{f}_i)$, which corresponds to the classes with the most similar semantics to the testing image:

$$\tilde{g}(\mathbf{f}_i)[k] = \begin{cases} g(\mathbf{f}_i)[k], & \text{if } g(\mathbf{f}_i)[k] \in \text{Top-}K_c(g(\mathbf{f}_i)), \\ -\infty, & \text{otherwise,} \end{cases} \quad (10)$$

where $\text{Top-}K_c(g(\mathbf{f}_i))$ denotes the top- K_c highest elements in $g(\mathbf{f}_i)$ and $K_c \ll K$. Subsequently, we derive the confidence score α_i^t of \mathbf{f}_i in belonging to task t for $t \leq t_c$, representing the amount of semantic information relevant to the input contained within each task:

$$\alpha_i^t = P_t(t|\mathbf{f}_i) = \frac{\sum_{k \in \mathcal{Y}^t} \exp(\tilde{g}(\mathbf{f}_i)[k]/\tau)}{\sum_{j=1}^{K_c} \exp(\tilde{g}(\mathbf{f}_i)[j]/\tau)}, \quad (11)$$

where τ is a temperature to control the smoothness of the task-confidence scores. Afterwards, the scores $\{\alpha_i^t\}_{t=1}^{t_c}$ serves as routing weights to aggregate task-specific intermediate features, forming a Mixture-of-Adapter (MoA) architecture. At the l -th block, given the input $\mathbf{X}_{i,l}$ of \mathbf{x}_i , the forward process is formulated as follows:

$$\begin{cases} [\hat{\mathbf{X}}_{i,l}, \hat{\mathbf{P}}_l] = \text{MSA}([\mathbf{X}_{i,l}; \mathbf{P}_l]), \\ \mathbf{X}_{i,l+1} = \text{FFN}(\hat{\mathbf{X}}_{i,l}) + \sum_{t=1}^T \alpha_i^t \mathcal{A}_l^t(\hat{\mathbf{X}}_{i,l}). \end{cases} \quad (12)$$

Compared to assigning a single task to each test image, such a Mixture-of-Adapters (MoA) structure avoids overconfident aggregation, further enhancing the model's robustness against misleading task-ids. The aggregated feature after the L -th block is utilized for final classification, denoted as $\hat{\mathbf{z}}_i = \mathcal{F}(\mathbf{x}_i; \mathcal{P}_{sh}, \{\mathcal{A}_{sp}^t\}_{t=1}^{t_c}, \{\alpha_i^t\}_{t=1}^{t_c})$. The final prediction \hat{k}_i is jointly determined by the global classifier g^u and the training classifier g :

$$\hat{k}_i = \arg \max_k \left[\frac{t_c}{t_c + 1} g^u(\hat{\mathbf{z}}_i)[k] + \frac{1}{t_c + 1} g(\hat{\mathbf{z}}_i)[k] \right]. \quad (13)$$

The inference of our CKA includes deriving the task-confidence scores through the task-shared network and aggregating task-specific knowledge through the proposed TC-MoA. The overall inference pipeline is illustrated in Alg.2.

Analysis of the working mechanism of TC-MoA. We visualize the top-1 confidence score distribution of samples with correct and incorrect task-ids in Fig.4 on 10S-ImageNetA. For a test sample \mathbf{x}_i^t from task t , its top-1 confidence score is denoted as $\alpha_i^{\hat{t}}$, where $\hat{t} = \arg \max_k \alpha_i^k$. For \mathbf{x}_i^t , if the predicted top-1 task matches its ground-truth task id, where $\hat{t} = t$, the sample is considered to have a correct prediction of task id.

As shown in Fig.4, samples with correct task-ids generally have higher top-1 scores. Therefore, for samples predicted with correct task-ids, TC-MoA assigns a single task-specific module with high confidence while neglecting others, acting as a **deterministic module selector**. For samples predicted with incorrect task-ids, TC-MoA adopts a **soft-label-like approach**, softly compensating for the incorrect modules through intermediate features from potential correct modules. Such a mechanism mitigates overconfidence in incorrect task-ids while preserving performance for correct ones, highlighting TC-MoA as a novel approach in handling incorrect task-ids in inference.

IV. EXPERIMENTS

Dataset and Evaluation Metrics. We evaluate our proposed method on four public CIL benchmarks, namely ImagenetR [64], ImagenetA [65], CIFAR100 [66] and DomainNet [67]. ImagenetR comprises 30000 images of 200 classes, which

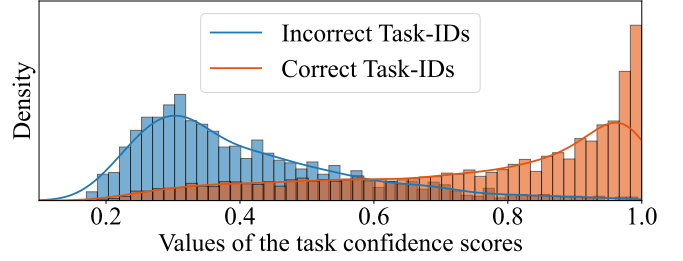


Fig. 4. Visualization of the distributions of the top-1 task-confidence scores.

share the same class names with Imagenet-21K [68] but belong to different domains. ImagenetA is a challenging dataset with 7500 images, which contains hard samples and exhibits significant class imbalance. Cifar100 is a commonly-used dataset in continual learning, which consists of 60000 32×32 images of 100 classes. DomainNet is a cross-domain dataset including images from 345 classes and 6 diverse domains. Following [3], [41], the 200 categories with the maximum number of images are selected for training and evaluation. We randomly split the datasets into 10 or 20 non-overlapping tasks. Note that for DomainNet, the 200 categories with the maximum number of images are selected for training and evaluation following [3], [41], [69].

Following existing PEFT-based CIL methods [2], [41], we evaluate the model performance through two commonly-used metrics: the accuracy of all classes after learning the last session (Last-acc), and the averaged accuracy of all incremental sessions (Avg-acc). We conduct all experiments under three different random seeds. The average performance and the maximum deviation are reported.

Implementation Details. Experiments are conducted on a single NVIDIA RTX 3090 GPU. We use ViT-B/16 [51] as our pre-trained backbone, which is pre-trained on ImageNet-21K [68]. The Adam optimizer with an initial learning rate of 0.01 is employed for training. We train each task for 100 epochs and the mini-batch is 110. Following [2], [3], [17], the PEFT modules are inserted into all transformer blocks to avoid searching. The prompt length is 4 and the middle dimensions of adapters are 64. In DKA, τ_f in Eq.4 is set to 0.05, τ_g and K_g in Eq.5 are 0.2 and 20. In TC-MoA, K_c in Eq.10 is set to 20 for ImageNetA and 10 for others, and τ in Eq.11 is set to 3.0.

A. Comparison with the State-of-the-Arts

We compare our CKA with state-of-the-art PEFT-based CIL methods, as shown in Tab.I, Tab.II and Tab.III. We compare our method with prompt-based methods [3], [16], [19], [20], adapter-based methods [2], [35], [54] and other PEFT-based methods [17], [55]. Tab.I shows the results of the standard 10-split incremental setting on four commonly-used benchmarks. Notably, our proposed method outperforms the state-of-the-art method SSAIT by 3.03%, 1.10%, 0.91%, and 1.61% in Last-acc on four datasets, respectively.

To further demonstrate the scalability of our method under long-term settings, we conduct experiments under the more challenging settings of 20, 50, and 100 tasks on ImagenetR, ImagenetA, and DomainNet. The results are shown in Tab.II

TABLE I

EXPERIMENTAL RESULTS ON FOUR CIL BENCHMARKS. WE REPORT THE AVERAGED RESULTS OVER 3 TRIALS. VPS-NSP[†] DENOTES OUR REPRODUCTION OF THE RESULTS UNDER THE SAME SETTINGS AND SEEDS IN OUR METHOD. THE HIGHEST RESULTS ARE IN **BOLD**, AND THE SECOND BEST RESULTS ARE UNDERLINED.

Method	Venue	10s-ImageNetR		10s-ImageNetA		10s-CIFAR100		10s-DomainNet	
		Last-acc \uparrow	Avg-acc \uparrow	Last-acc \uparrow	Avg-acc \uparrow	Last-acc \uparrow	Avg-acc \uparrow	Last-acc \uparrow	Avg-acc \uparrow
L2P [16]	CVPR-22	72.34 \pm 0.17	77.36 \pm 0.64	44.04 \pm 0.93	51.24 \pm 2.26	84.06 \pm 0.88	88.26 \pm 1.34	81.17 \pm 0.83	87.43 \pm 0.95
DualPrompt [19]	ECCV-22	69.10 \pm 0.62	74.28 \pm 0.66	53.19 \pm 0.74	64.59 \pm 0.08	86.93 \pm 0.24	91.13 \pm 0.32	81.70 \pm 0.78	87.80 \pm 0.99
ADA [35]	NIPS-22	73.76 \pm 0.27	79.57 \pm 0.84	50.16 \pm 0.20	59.43 \pm 2.20	88.25 \pm 0.26	91.85 \pm 1.32	—	—
CODAPrompt [20]	CVPR-23	73.31 \pm 0.50	78.47 \pm 0.53	52.08 \pm 0.12	63.92 \pm 0.12	83.21 \pm 3.39	87.71 \pm 3.17	80.04 \pm 0.79	86.27 \pm 0.82
LAE [53]	ICCV-23	72.29 \pm 0.14	77.99 \pm 0.46	47.18 \pm 1.17	58.15 \pm 0.73	85.25 \pm 0.43	89.80 \pm 1.20	—	—
SLCA [40]	ICCV-23	79.35 \pm 0.28	83.29 \pm 0.46	61.05 \pm 0.63	68.88 \pm 2.31	91.26 \pm 0.37	94.29 \pm 0.92	—	—
Adam-adapter [54]	IJCV-24	65.79 \pm 0.98	72.42 \pm 1.41	48.81 \pm 0.08	58.84 \pm 1.37	87.29 \pm 0.27	91.21 \pm 1.33	—	—
RAPF [55]	ECCV-24	79.62	86.28	—	—	79.04	86.19	—	—
InfLoRA [17]	CVPR-24	75.65 \pm 0.14	80.82 \pm 0.24	47.04 \pm 0.90	56.91 \pm 1.27	86.51 \pm 0.73	91.70 \pm 0.32	81.45 \pm 0.68	—
EASE [21]	CVPR-24	71.43 \pm 0.18	78.04 \pm 0.67	59.25 \pm 0.88	68.92 \pm 2.06	85.71 \pm 0.76	90.96 \pm 0.83	—	—
CPrompt [41]	CVPR-24	77.14 \pm 0.11	82.92 \pm 0.70	55.15 \pm 0.85	65.49 \pm 0.52	87.82 \pm 0.21	92.53 \pm 0.23	82.97 \pm 0.34	88.54 \pm 0.41
SSIAT [2]	CVPR-24	79.38 \pm 0.59	83.63 \pm 0.43	<u>62.43</u> \pm 1.63	70.83 \pm 1.63	<u>91.35</u> \pm 0.26	<u>94.35</u> \pm 0.60	<u>85.11</u> \pm 0.56	<u>89.80</u> \pm 0.34
VQ-Prompt [56]	NeurIPS-24	78.71 \pm 0.22	83.24 \pm 0.68	—	—	88.73 \pm 0.27	92.84 \pm 0.73	—	—
VPT-NSP [†] [3]	NeurIPS-24	77.95 \pm 0.22	83.44 \pm 0.40	53.83 \pm 0.37	63.93 \pm 1.08	90.19 \pm 0.43	94.12 \pm 1.05	83.05 \pm 1.06	87.83 \pm 0.92
DIA [57]	CVPR-25	79.03	85.61	61.69	<u>71.58</u>	90.80	94.29	—	—
ACMap [58]	CVPR-25	70.49	77.31	56.19	65.19	87.81	92.04	—	—
SEMA [59]	CVPR-25	78.00	83.56	53.32	64.53	86.98	91.37	—	—
LoRA-DRS [60]	CVPR-25	74.74 \pm 0.78	81.16 \pm 0.59	—	—	89.14 \pm 0.23	92.55 \pm 0.25	—	—
CL-LoRA [61]	CVPR-25	—	—	60.54 \pm 0.63	70.15 \pm 2.23	85.32 \pm 0.08	91.02 \pm 0.12	—	—
CKAA (Ours)	—	82.41 \pm 0.13	87.20 \pm 0.35	63.53 \pm 0.66	71.11 \pm 1.03	92.26 \pm 0.39	95.18 \pm 0.86	86.72 \pm 0.55	90.68 \pm 0.78

TABLE II

EXPERIMENTAL RESULTS UNDER THE LONG-TERM SETTING (20 INCREMENTAL TASKS) ON IMAGENETR AND IMAGENETA.

Method	20s-ImageNetR		20s-ImageNetA	
	Last-acc \uparrow	Avg-acc \uparrow	Last-acc \uparrow	Avg-acc \uparrow
L2P [16]	69.64 \pm 0.42	75.28 \pm 0.57	40.48 \pm 1.78	49.62 \pm 1.46
DualPrompt [19]	66.61 \pm 0.58	72.45 \pm 0.37	42.28 \pm 1.94	53.39 \pm 1.64
CODAPrompt [20]	69.96 \pm 0.50	75.34 \pm 0.85	44.62 \pm 1.92	54.86 \pm 0.50
LAE [53]	69.86 \pm 0.43	77.38 \pm 0.61	39.52 \pm 0.78	51.75 \pm 2.15
SLCA [40]	74.63 \pm 1.55	79.92 \pm 1.29	36.69 \pm 21.31	56.35 \pm 7.09
Adam-adapter [54]	57.42 \pm 0.84	64.75 \pm 0.79	48.65 \pm 0.12	59.55 \pm 1.07
InfLoRA [17]	71.01 \pm 0.45	77.28 \pm 0.45	—	—
CPrompt [41]	74.79 \pm 0.28	81.46 \pm 0.93	—	—
SSIAT [2]	75.67 \pm 0.14	82.30 \pm 0.36	59.16 \pm 1.03	68.45 \pm 1.92
VPT-NSP [†] [3]	75.69 \pm 0.61	81.87 \pm 0.59	49.81 \pm 1.29	61.41 \pm 1.84
DIA [57]	76.32	83.51	—	—
CKAA (Ours)	80.98 \pm 0.54	86.28 \pm 0.18	60.54 \pm 0.50	70.55 \pm 0.64

TABLE III

EXPERIMENTAL RESULTS UNDER THE LONG-TERM SETTING (50 & 100 TASKS) ON IMAGENETR AND DOMAINNET. LAST-ACC IS REPORTED.

Method	S-ImageNetR		S-DomainNet	
	50s	100s	50s	100s
L2P [16]	51.38	41.51	63.13	54.83
OVOR-Deep [62]	63.25	43.02	68.29	52.09
ConvPrompt [63]	64.61	44.32	71.76	56.21
InfLoRA [17]	62.81	42.23	<u>71.87</u>	48.06
CPrompt [41]	70.75	59.90	70.74	57.60
EASE [21]	70.27	51.56	65.34	37.56
VPT-NSP [†] [3]	69.48	62.23	71.28	57.35
CKAA (Ours)	78.20 \pm 0.65	73.41 \pm 0.51	81.53 \pm 2.60	77.28 \pm 3.09

and Tab.III. Under the 20-split setting, our method outperforms SSIAT by 5.31% and 1.38% in Last-acc on two datasets. While under the 50-split and 100-split settings, our proposed CKAA exhibits superior performances, which surpasses VPT-NSP by 8.71% and 11.18% in Last-Acc on the ImageNetR dataset. For the 50-split and 100-split settings, the intermediate dimensions of adapters are set to 16 and 8 to avoid additional inference overhead. The results highlight its scalability and remarkable ability to address catastrophic forgetting in long-term CIL problems.

To sum up, our proposed method has two main advantages:

(1) CKAA significantly enhances the model's robustness against misleading task-ids, which is crucial for CIL frameworks with task-specific design; (2) CKAA is particularly well-suited for long sequence tasks, as it seamlessly integrates new knowledge regardless of task numbers.

B. Comparison with Existing Methods on Fine-Grained Datasets

We evaluate our method on the fine-grained datasets CUB-200 [71] and StanfordCars [72] to demonstrate its effectiveness in fine-grained CIL classification. CUB-200 [71] contains 11,788 images of 200 bird species with fine-grained class labels. StanfordCars [72] is a fine-grained car dataset including

TABLE IV

EXPERIMENTAL RESULTS ON 10S-CUB-200.

Method	Venue	Last-acc \uparrow	Avg-acc \uparrow
L2P [16]	CVPR-22	67.02 \pm 1.90	79.62 \pm 1.60
DualPrompt [19]	ECCV-22	68.48 \pm 0.47	80.59 \pm 1.50
CODAPrompt [20]	CVPR-23	77.23 \pm 1.12	81.90 \pm 0.85
LAE [53]	ICCV-23	80.97 \pm 0.51	87.22 \pm 1.21
SLCA [40]	ICCV-23	84.68 \pm 0.09	90.77 \pm 0.79
Adam-adapter [54]	IJCV-24	85.84 \pm 0.08	91.33 \pm 0.49
EASE [21]	CVPR-24	86.81	92.23
SSIAT [2]	CVPR-24	88.75 \pm 0.38	93.00 \pm 0.90
VPT-NSP [†] [3]	NIPS-24	83.08 \pm 0.75	90.32 \pm 0.62
CoFiMA [70]	ECCV-24	87.11 \pm 0.56	91.87 \pm 0.69
DIA [57]	CVPR-25	86.73	93.21
ACMap [58]	CVPR-25	86.66	91.56
CKAA (Ours)	—	89.48 \pm 0.46	93.34 \pm 0.26

TABLE V

EXPERIMENTAL RESULTS ON 10S-STANFORDCARS.

Method	Venue	Last-acc \uparrow	Avg-acc \uparrow
L2P [16]	CVPR-22	60.39 \pm 1.99	71.92 \pm 1.12
DualPrompt [19]	ECCV-22	57.27 \pm 0.34	70.36 \pm 2.33
ESN [69]	AAAI-23	56.91 \pm 0.56	72.82 \pm 0.79
CODAPrompt [20]	CVPR-23	62.24 \pm 0.14	73.28 \pm 0.93
CPrompt [41]	CVPR-24	66.77 \pm 0.37	<u>76.81</u> \pm 0.27
CKAA (Ours)	—	80.92 \pm 0.08	87.32 \pm 0.90

TABLE VI
ABLATION STUDIES OF EACH COMPONENT IN OUR PROPOSED METHOD ON IMAGENETR AND IMAGENETA.

Idx	\mathcal{P}_{sh}	TC-MoA	FA	CA	10s-ImageNetR		10s-ImageNetA		20s-ImageNetR	
					Last-acc \uparrow	Avg-acc \uparrow	Last-acc \uparrow	Avg-acc \uparrow	Last-acc \uparrow	Avg-acc \uparrow
CKAA with frozen pre-trained task-shared network.										
1	—	—	—	—	65.65 \pm 0.58	72.82 \pm 0.67	46.01 \pm 0.92	56.51 \pm 0.70	63.67 \pm 0.68	71.56 \pm 1.14
2	—	✓	—	—	76.72 \pm 0.61	83.14 \pm 0.32	53.92 \pm 0.85	64.16 \pm 0.18	73.91 \pm 0.35	81.15 \pm 0.32
3	—	✓	✓	—	78.54 \pm 0.39	84.36 \pm 0.28	57.12 \pm 1.75	65.68 \pm 0.25	75.58 \pm 0.19	82.43 \pm 0.76
4	—	✓	—	✓	79.77 \pm 0.12	85.09 \pm 0.24	59.71 \pm 0.20	68.55 \pm 0.32	78.65 \pm 0.27	84.52 \pm 0.41
5	—	✓	✓	✓	81.56 \pm 0.13	86.63 \pm 0.13	62.49 \pm 1.53	70.59 \pm 0.56	79.86 \pm 0.32	85.33 \pm 0.52
CKAA with learnable visual prompt-based task-shared network.										
6	✓	—	—	—	77.95 \pm 0.22	83.44 \pm 0.40	53.83 \pm 0.37	63.93 \pm 1.08	75.69 \pm 0.62	81.87 \pm 0.56
7	✓	✓	—	—	79.14 \pm 0.21	85.04 \pm 0.33	54.33 \pm 0.87	64.43 \pm 1.22	76.88 \pm 0.57	82.91 \pm 0.52
8	✓	✓	✓	—	79.74 \pm 0.34	85.29 \pm 0.19	58.13 \pm 0.20	66.59 \pm 0.84	77.82 \pm 0.55	83.71 \pm 0.39
9	✓	✓	—	✓	81.80 \pm 0.38	86.59 \pm 0.18	61.29 \pm 0.46	69.31 \pm 1.16	80.18 \pm 0.42	85.75 \pm 0.24
10	✓	✓	✓	✓	82.41 \pm 0.13	87.20 \pm 0.35	63.53 \pm 0.66	71.11 \pm 1.03	80.98 \pm 0.35	86.28 \pm 0.18

TABLE VII
ABLATION STUDIES OF VARIOUS TASK-SPECIFIC KNOWLEDGE AGGREGATION STRATEGIES WITHOUT AND WITH DKA ON TWO DATASETS.

Method	10s-ImageNetR		10s-ImageNetA	
	Last-acc \uparrow	Avg-acc \uparrow	Last-acc \uparrow	Avg-acc \uparrow
<i>Without Dual-level Knowledge Alignment (DKA)</i>				
Query-key	74.60 \pm 0.58	80.75 \pm 0.82	47.30 \pm 0.88	58.21 \pm 0.76
Maximum	77.03 \pm 0.46	82.95 \pm 0.98	49.18 \pm 0.72	59.57 \pm 1.43
TC-MoA	79.14 \pm 0.21	85.04 \pm 0.33	54.33 \pm 0.87	64.43 \pm 1.22
<i>With Dual-level Knowledge Alignment (DKA)</i>				
Query-key	76.02 \pm 0.45	81.88 \pm 0.67	56.39 \pm 0.37	65.80 \pm 1.28
Maximum	78.55 \pm 0.25	84.20 \pm 0.72	58.12 \pm 0.57	67.53 \pm 0.56
TC-MoA	82.41 \pm 0.13	87.20 \pm 0.35	63.53 \pm 0.66	71.11 \pm 1.03

TABLE VIII
ABLATION STUDIES OF FEATURE SIMULATION ON 10S-IMAGENETA.

Method	Last-acc \uparrow	Avg-acc \uparrow
CKAA (Ours)	63.53 \pm 0.66	71.11 \pm 1.03
<i>The following methods are based on FA and TC-MoA.</i>		
CKAA w/o CA	58.13 \pm 0.20	66.59 \pm 0.84
+ CA w/o subspace transfer	62.38 \pm 0.70	70.35 \pm 1.28
+ CA w/o affinities G	63.20 \pm 0.63	70.83 \pm 0.92

196 classes and 16185 car images. Following existing methods [2], [41], [54], we evaluate our method under the 10-split setting. The experiment results on CUB-200 and StanfordCars are outlined in Tab.IV and Tab.V, respectively. Our method exhibits superior performance, outperforming the state-of-the-art SSIAT by 0.73% Last-acc on CUB-200 and 14.15% Last-acc on StanfordCars. The results demonstrate the robustness of our proposed CKAA against the catastrophic forgetting of fine-grained knowledge.

C. Ablation Study

In this subsection, we perform ablation studies on the components of our framework on ImageNetR and ImageNetA datasets with 10- or 20-split tasks, as shown in Tab.VI. We also visualize the task-by-task accuracy changing curves of the ablation studies on four benchmarks with 10- or 100-split tasks, as shown in Fig.5. Our baseline is the frozen ViT backbone with a trainable classifier (Idx 1) and Fig.5.

The effectiveness of \mathcal{P}_{sh} . We conduct experiments on the learnable visual prompt-based task-shared network to demonstrate its effectiveness. Specifically, we directly replace the learnable task-shared network with the frozen pre-trained backbone. As indicated in Tab.VI, the learnable visual prompts \mathcal{P}_{sh} improves the model’s Last-acc by 0.85% and Avg-acc by

0.57% on 10s-ImagenetR (Idx 5 *v.s.* Idx 10). This improvement is mainly due to the learnable task-shared network’s ability to capture common knowledge across downstream datasets, compared to a frozen pre-trained backbone. It results in more precise task identification during inference and more appropriate routing weights for aggregating task-specific knowledge in TC-MoA.

The effectiveness of DKA. The proposed DKA (FA & CA) yields an overall improvement of 3.27%~9.20% on Last-acc compared to the independent training of sub-modules. The Feature-level Alignment (FA) improves the performance by 0.60%~3.80% Last-acc (Idx 7 *v.s.* Idx 8). Our FA effectively aligns feature semantics within different subspaces, resulting in a performance gain. The Classifier-level Alignment (CA) further substantially improves the model performance of 2.67%~5.40% on Last-acc (Idx 8 *v.s.* Idx 10). Unlike existing methods that use features with the proper task-ids to train the classifier, our CA simulates the wrongly projected features to train a unified classifier, improving the classifier’s robustness.

Tab.VII further shows the performance *without and with DKA under various task-specific knowledge aggregation strategies*. In Tab.VII, “Query-key” matching designs a task-key for each task-specific sub-module and selects the adapter corresponding to the task-key with the highest similarity to the input for integrating task-specific knowledge, which is a widely-used technology in PEFT-based CIL methods [16], [19], [20], [41], [73]. “Maximum” selection directly selects the sub-module with the highest task-confidence score, representing a one-hot variant of our TC-MoA. The results (upper *vs.* lower in Tab.VII) indicate that DKA gains model performance with various aggregation strategies, further demonstrating the effectiveness of our DKA.

To gain a more detailed understanding of our CA, we conduct ablation studies of *the feature simulation process* in CA on 10s-ImageNetA to indicate its efficacy, as shown in Tab.VIII. “CA w/o subspace transfer” denotes training the classifier using features obtained directly from Gaussian Sampling without subspace transfer. “CA w/o affinities **G**” denotes modeling the shift of previous features without considering their affinities **G** with current features, instead directly utilizing the average shift of current features. The results demonstrate the efficacy of each step in our affinity-guided feature simulation.

Additionally, we examine the effectiveness of our DKA

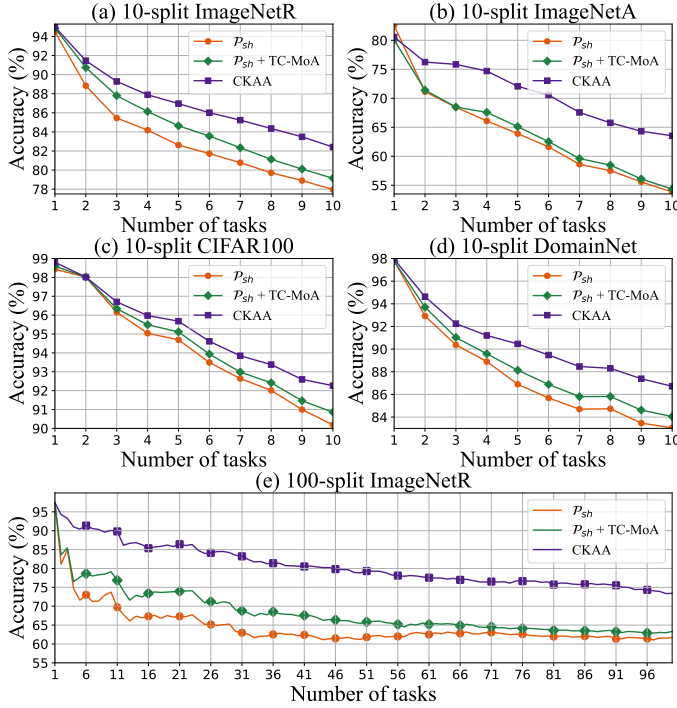


Fig. 5. The task-by-task accuracy changing curves of our baseline (P_{sh}), $P_{sh}+TC-MoA$ and CKAA on four benchmarks.

through the task-by-task accuracy curves in Fig.5, highlighting DKA's superiority under long-term settings.

The effectiveness of TC-MoA. TC-MoA achieves an improvement of 0.50%~1.19% Last-acc (Idx 6 *v.s.* Idx 7) compared to directly utilizing the task-shared network for classification. This observation indicates that our TC-MoA is a powerful tool for aggregating task-specific knowledge, while the task-shared network alone is insufficient for the final decision. We further compare *different aggregation strategies* in Tab.VII, where existing “Query-Key” matching exhibits limited performance as a single task key is insufficient to represent the data distribution within an entire task. In contrast, our TC-MoA softly aggregates task-specific knowledge based on task-confidence scores, avoiding overconfidence in misleading task-ids and fully leveraging the fine-grained instance-class relationships.

D. Experiments under various pre-trained models

We also conduct experiments on 10s-ImageNetR with ViT-B/16 under various self-supervised pre-training methods, including DINO [76] and iBOT [77], following [17], [75]. The results are shown in Tab.IX, which exhibit a performance degradation with a self-supervised pre-trained backbone compared to utilizing a backbone pre-trained in a supervised manner. However, our proposed method still outperforms existing PEFT-based methods. The results demonstrate that our approach can be adapted to models with various pre-training schemes, highlighting its generalizability.

E. Parameter Analysis

We conduct experiments to analyze the impact of the hyper-parameters in our proposed method on 10s-ImageNetR and

TABLE IX
RESULTS OF EXISTING METHODS UNDER VARIOUS PRE-TRAINED MODELS. HERE, DINO-1K AND iBOT-1K DENOTE THAT THE FROZEN BACKBONE IS PRE-TRAINED ON IMAGENET-1K THROUGH DINO AND iBOT PRE-TRAINING ALGORITHMS, RESPECTIVELY.

PTM	Method	Last-acc \uparrow	Avg-acc \uparrow
DINO-1k	L2P [16]	56.71 \pm 0.12	63.59 \pm 0.21
	DualPrompt [19]	60.23 \pm 0.42	66.57 \pm 0.25
	CODAPrompt [20]	64.02 \pm 0.68	71.50 \pm 0.42
	C-LoRA [74]	63.07 \pm 0.36	68.09 \pm 0.41
	LAE [53]	61.03 \pm 0.27	69.89 \pm 0.15
	HiDe-Prompt [75]	68.11 \pm 0.18	71.70 \pm 0.01
	InfLoRA [17]	68.31 \pm 0.28	76.15 \pm 0.05
	VPS-NSP [†] [3]	68.96 \pm 0.94	76.22 \pm 0.56
	CKAA (Ours)	75.19\pm0.29	81.17\pm0.21
iBOT-1k	L2P [16]	60.80 \pm 0.35	66.58 \pm 0.28
	DualPrompt [19]	63.78 \pm 0.38	68.88 \pm 0.16
	CODAPrompt [20]	68.02 \pm 0.48	74.28 \pm 0.47
	C-LoRA [74]	68.60 \pm 0.07	73.47 \pm 0.28
	LAE [53]	64.14 \pm 0.29	72.59 \pm 0.22
	HiDe-Prompt [75]	71.33 \pm 0.21	73.62 \pm 0.13
	InfLoRA [17]	71.84 \pm 0.09	78.29 \pm 0.09
	VPS-NSP [†] [3]	73.25 \pm 0.78	79.65 \pm 0.63
	CKAA (Ours)	77.96\pm0.22	83.26\pm0.15

10s-ImageNetA benchmarks, including τ_f in Eq.4, K_g and τ_g in Eq.5, K_c in Eq.10 and τ in Eq.11.

We first analyze the hyper-parameters in TC-MoA, including K_c and τ . The results are shown in Fig.6(a) and Fig.6(b). K_c is designed to select the Top- K_c classes with the highest logits to compute the task-confidence scores. τ is a temperature factor designed to control the smoothness of the scores. We set $K_c = 10$ for ImageNetR and $K_c = 20$ for ImageNetA, $\tau = 2.0$ for all datasets based on experimental results.

Then we analyze the hyper-parameters in DKA, including τ_f , K_g , and τ_g . The results are shown in Fig.6(c), Fig.6(d), and Fig.6(e). τ_f is a temperature factor of the Cross Subspace Feature Alignment (CSFA) loss in Eq.4. K_g and τ_g are two parameters for modeling the affinities between current and previous data. Based on the experimental results, we set $\tau_f = 0.05$, $K_g = 20$ and $\tau_g = 0.2$ for all datasets.

F. Analysis of the Effectiveness of CKAA in handling Misleading Task-ids

We conduct ablation studies on 10s-ImageNetA to analyze the effectiveness of our proposed CKAA in enhancing the model's robustness against misleading task-ids. Specifically, we divide the testing samples into two subsets: (1) **Challenging samples**: These are misclassified by the task recognizer and assigned with incorrect task-ids; (2) **Easy samples**: These are classified correct task-ids. We report the task-by-task accuracy of these two types of samples, respectively. The results are shown in Tab.X and Tab.XI.

As shown in Tab.X, the proposed TC-MoA and DKA effectively improve the prediction accuracy for the challenging samples, delivering more reliable predictions for features under incorrect task-specific sub-modules. Notably, the accuracy in the half bottom of Tab.X is lower compared to the top half part. It is mainly due to our learnable task-shared network (the half bottom) encapsulates sufficient downstream information, the samples it fails to distinguish are inherently more challenging. Overall, our CKAA achieves significant improvement in the classification accuracy of these challenging samples.

TABLE X
TASK-BY-TASK ACCURACY OF THE *challenging samples* ON 10S-IMAGENETA.

Methods	Ses.2	Ses.3	Ses.4	Ses.5	Ses.6	Ses.7	Ses.8	Ses.9	Ses.10
<i>CKAA with frozen pre-trained task-shared network.</i>									
pre-trained backbone	0.00 \pm 0.00	0.00 \pm 0.00	0.00 \pm 0.00	0.00 \pm 0.00	0.00 \pm 0.00	0.00 \pm 0.00	0.00 \pm 0.00	0.00 \pm 0.00	0.00 \pm 0.00
+ TC-MoA	43.26 \pm 5.96	44.84 \pm 5.08	43.67 \pm 1.45	39.47 \pm 2.20	36.09 \pm 2.26	35.01 \pm 2.87	32.29 \pm 1.01	31.00 \pm 1.75	30.20 \pm 1.46
+ TC-MoA + CA	52.20 \pm 2.80	51.74 \pm 4.33	48.49 \pm 1.28	46.61 \pm 1.56	43.99 \pm 1.64	41.93 \pm 2.53	40.51 \pm 0.51	39.19 \pm 0.41	37.88 \pm 0.47
+ TC-MoA + FA	43.72 \pm 7.96	48.07 \pm 7.06	47.08 \pm 2.65	43.17 \pm 2.16	41.81 \pm 2.52	37.80 \pm 3.44	36.68 \pm 3.04	34.73 \pm 1.53	33.76 \pm 1.24
+ TC-MoA + DKA	53.99 \pm 6.41	53.06 \pm 2.95	52.60 \pm 1.86	49.65 \pm 0.27	47.33 \pm 2.52	45.11 \pm 2.82	44.54 \pm 0.87	42.87 \pm 0.89	42.01 \pm 0.66
<i>CKAA with learnable visual prompt-based task-shared network.</i>									
\mathcal{P}_{sh}	0.00 \pm 0.00	0.00 \pm 0.00	0.00 \pm 0.00	0.00 \pm 0.00	0.00 \pm 0.00	0.00 \pm 0.00	0.00 \pm 0.00	0.00 \pm 0.00	0.00 \pm 0.00
+ TC-MoA	23.90 \pm 5.54	19.97 \pm 1.67	17.62 \pm 1.23	14.82 \pm 2.42	13.29 \pm 1.13	12.31 \pm 0.33	12.48 \pm 1.05	11.41 \pm 0.5	10.48 \pm 0.22
+ TC-MoA + CA	30.48 \pm 5.96	29.59 \pm 0.88	30.80 \pm 6.53	28.56 \pm 5.17	27.54 \pm 2.62	27.36 \pm 3.25	25.97 \pm 1.60	25.50 \pm 1.08	25.68 \pm 0.39
+ TC-MoA + FA	20.96 \pm 4.42	21.41 \pm 4.48	21.95 \pm 3.96	19.60 \pm 2.12	17.94 \pm 1.73	17.59 \pm 3.21	17.25 \pm 2.05	16.81 \pm 1.57	16.43 \pm 1.52
+ TC-MoA + DKA	35.76 \pm 0.93	33.75 \pm 8.83	36.02 \pm 2.03	31.84 \pm 2.85	31.28 \pm 2.78	29.91 \pm 2.85	29.25 \pm 1.42	28.31 \pm 1.97	27.71 \pm 0.53

TABLE XI
TASK-BY-TASK ACCURACY OF THE *easy samples* ON 10S-IMAGENETA.

Methods	Ses.2	Ses.3	Ses.4	Ses.5	Ses.6	Ses.7	Ses.8	Ses.9	Ses.10
<i>CKAA with frozen pre-trained task-shared network.</i>									
pre-trained backbone	67.05 \pm 3.05	67.15 \pm 0.96	69.63 \pm 1.68	71.60 \pm 2.15	72.61 \pm 3.42	73.43 \pm 2.46	74.12 \pm 1.52	72.56 \pm 1.93	72.57 \pm 1.84
+ TC-MoA	79.50 \pm 3.98	82.11 \pm 3.68	82.65 \pm 1.49	83.54 \pm 1.81	82.73 \pm 0.99	82.48 \pm 0.69	82.91 \pm 2.30	82.53 \pm 1.06	82.41 \pm 1.36
+ TC-MoA + CA	81.92 \pm 2.65	85.46 \pm 1.61	86.08 \pm 1.03	87.17 \pm 1.66	87.25 \pm 1.13	86.24 \pm 0.63	86.09 \pm 1.34	85.92 \pm 1.70	86.36 \pm 1.68
+ TC-MoA + FA	81.07 \pm 3.75	82.75 \pm 3.30	82.68 \pm 1.20	84.89 \pm 0.40	83.85 \pm 1.63	84.49 \pm 1.52	84.97 \pm 0.86	84.76 \pm 2.38	84.35 \pm 2.39
+ TC-MoA + DKA	83.12 \pm 1.31	86.40 \pm 1.86	86.19 \pm 0.99	88.81 \pm 1.34	87.79 \pm 1.34	86.78 \pm 0.75	86.89 \pm 2.12	86.87 \pm 2.89	86.83 \pm 3.30
<i>CKAA with learnable visual prompt-based task-shared network.</i>									
\mathcal{P}_{sh}	81.92 \pm 2.49	83.42 \pm 2.79	85.05 \pm 3.00	85.80 \pm 2.99	85.86 \pm 2.48	85.14 \pm 1.72	85.79 \pm 1.49	85.45 \pm 1.79	85.98 \pm 1.17
+ TC-MoA	79.01 \pm 3.99	80.84 \pm 2.24	83.49 \pm 4.47	84.31 \pm 1.51	84.60 \pm 1.27	83.62 \pm 0.48	83.07 \pm 0.64	82.33 \pm 1.43	82.85 \pm 1.97
+ TC-MoA + CA	80.10 \pm 9.33	84.19 \pm 3.20	86.26 \pm 3.78	85.54 \pm 1.66	86.09 \pm 1.42	86.64 \pm 3.07	86.84 \pm 0.39	85.71 \pm 0.49	85.76 \pm 0.50
+ TC-MoA + FA	80.22 \pm 1.81	82.35 \pm 2.26	84.26 \pm 0.55	85.22 \pm 1.74	85.30 \pm 1.09	85.02 \pm 2.25	83.91 \pm 1.05	84.34 \pm 1.93	83.49 \pm 2.56
+ TC-MoA + DKA	82.81 \pm 4.11	85.13 \pm 1.71	86.95 \pm 2.04	87.76 \pm 2.66	88.07 \pm 1.11	87.39 \pm 1.38	87.23 \pm 0.85	86.08 \pm 0.81	86.51 \pm 0.52

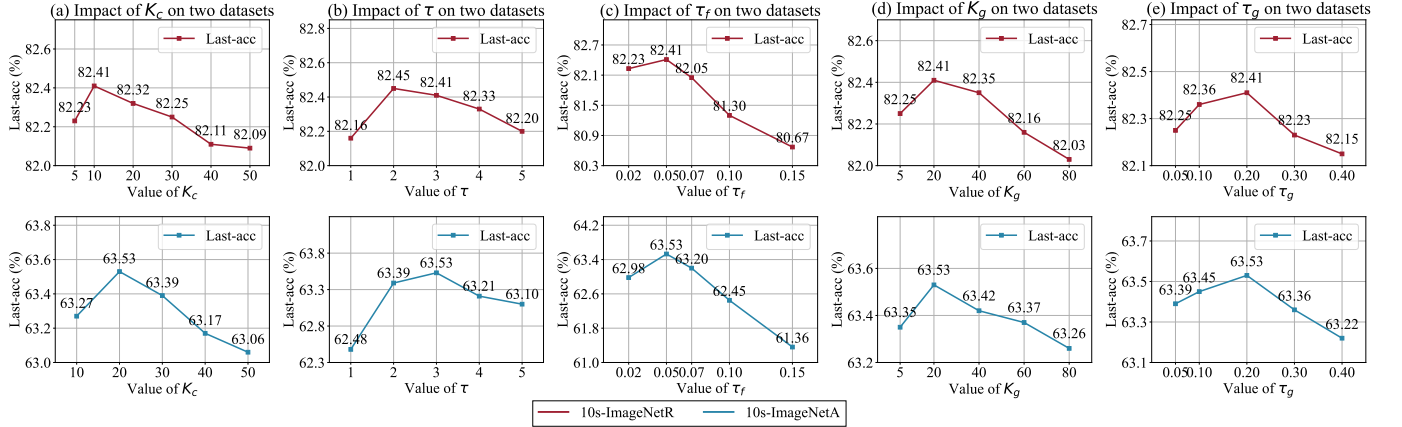


Fig. 6. Parameter analysis of K_c and τ in TC-MoA, and τ_f , K_g and τ_g in DKA on 10S-ImageNetR and 10S-ImageNetA.

G. Analysis of additional computational costs

We conduct experiments to analyze the impact of adapter widths on 10s-ImageNetA and 10s-ImageNetR datasets, the results are shown in Tab.XII. Decreasing the adapter width results in slight performance degradation on 10s-ImageNetR, while it exhibits negligible impact on the performance of 10s-ImageNetA. Notably, our method performs well even with a width of 2, referred to as ‘CKAA-’.

We further report additional computational cost per image per task in Tab.XIII. Since the task-specific modules and the classifier are expanded during learning of new tasks, the computational costs exhibit a slight growth. Despite the growth, the added parameters are negligible (+0.06% per task with adapter width 2 in CKAA-), yet strong performance is retained. We report the training cost of per batch at different stages in Tab.XIV. CKAA introduces negligible additional cost

even in long-term tasks (+0.026% in T=100): The feature-level alignment caches features from previous modules once at the beginning of each session, avoiding extra training cost; and the classifier-level alignment operates solely at the classifier level without involving heavy backbone computation.

V. CONCLUSION

In this paper, we propose the Cross-subspace Knowledge Alignment and Aggregation (CKAA) framework to resolve feature subspace misalignment and improve model robustness against misleading task-ids. During training, CKAA introduces Dual-level Knowledge Alignment (DKA), which aligns feature semantics and unifies decision boundaries across task-specific subspaces, addressing the misalignment issue caused by independent sub-module training. During inference, CKAA

TABLE XII
MODEL PERFORMANCE UNDER DIFFERENT ADAPTER WIDTHS.

Width	Params	Flops	10s-ImageNetA		10s-ImageNetR	
			Last-acc \uparrow	Avg-acc \uparrow	Last-acc \uparrow	Avg-acc \uparrow
2	0.42M (0.48%)	17.09GMac	63.40 \pm 0.66	71.84 \pm 0.46	81.63 \pm 0.70	86.93 \pm 0.04
4	0.83M (0.96%)	17.16GMac	63.84 \pm 0.47	72.15 \pm 0.76	82.04 \pm 0.20	87.02 \pm 0.07
8	1.66M (1.93%)	17.31GMac	64.03 \pm 1.06	72.09 \pm 0.14	81.77 \pm 0.75	86.96 \pm 0.07
16	3.32M (3.86%)	17.60GMac	63.56 \pm 0.32	71.27 \pm 1.15	82.06 \pm 1.09	87.03 \pm 0.35
32	6.64M (7.72%)	18.18GMac	63.27 \pm 0.74	71.33 \pm 1.13	82.15 \pm 0.47	87.21 \pm 0.13
64	13.28M (15.44%)	19.34GMac	63.53 \pm 0.66	71.11 \pm 1.03	82.41 \pm 0.13	87.20 \pm 0.35

TABLE XIII
ADDITIONAL MEMORY AND COMPUTATIONAL COST PER TASK.

Method	Memory	Computational Cost	10S-ImageNetA	
			Last-acc \uparrow	Avg-acc \uparrow
\mathcal{P}_{sh} (Baseline)	86M	17.00GMac	53.83 \pm 0.37	63.93 \pm 1.08
CKAA- ($w = 2$)	+0.04M (0.05%)	+0.01GMac (+0.06%)	63.40 \pm 0.66	71.84 \pm 0.46
CKAA ($w = 64$)	+1.33M (1.55%)	+0.23GMac (+1.35%)	63.53 \pm 0.66	71.11 \pm 1.03

TABLE XIV
ADDITIONAL TRAINING COST AT DIFFERENT INCREMENTAL STAGES.

Task Index T	T = 0 (Base)	T = 25	T = 50	T = 75	T = 100
Training Cost (GMac)	1880.48	1880.51	1880.61	1880.77	1880.98
Increase Rate (%)	–	+0.002%	+0.007%	+0.015%	+0.026%

designs Task-Confidence-guided Mixture of Adapters (TC-MoA), a dynamic aggregation scheme that softly combines task-specific knowledge based on confidence scores, mitigating overconfidence in erroneous task-id predictions.

REFERENCES

- [1] S.-A. Rebuffi, A. Kolesnikov, G. Sperl, and C. H. Lampert, “icarl: Incremental classifier and representation learning,” in *Proceedings of the IEEE conference on Computer Vision and Pattern Recognition*, 2017, pp. 2001–2010.
- [2] Y. Tan, Q. Zhou, X. Xiang, K. Wang, Y. Wu, and Y. Li, “Semantically-shifted incremental adapter-tuning is a continual vitransformer,” in *Proceedings of the IEEE/CVF Conference on Computer Vision and Pattern Recognition*, 2024, pp. 23 252–23 262.
- [3] Y. Lu, S. Zhang, D. Cheng, Y. Xing, N. Wang, P. Wang, and Y. Zhang, “Visual prompt tuning in null space for continual learning,” *arXiv preprint arXiv:2406.05658*, 2024.
- [4] J. Kirkpatrick, R. Pascanu, N. Rabinowitz, J. Veness, G. Desjardins, A. A. Rusu, K. Milan, J. Quan, T. Ramalho, A. Grabska-Barwinska *et al.*, “Overcoming catastrophic forgetting in neural networks,” *Proceedings of the national academy of sciences*, vol. 114, no. 13, pp. 3521–3526, 2017.
- [5] Z. Li and D. Hoiem, “Learning without forgetting,” *IEEE transactions on pattern analysis and machine intelligence*, vol. 40, no. 12, pp. 2935–2947, 2017.
- [6] S.-W. Lee, J.-H. Kim, J. Jun, J.-W. Ha, and B.-T. Zhang, “Overcoming catastrophic forgetting by incremental moment matching,” *Advances in neural information processing systems*, vol. 30, 2017.
- [7] M. McCloskey and N. J. Cohen, “Catastrophic interference in connectionist networks: The sequential learning problem,” in *Psychology of learning and motivation*. Elsevier, 1989, vol. 24, pp. 109–165.
- [8] A. Soutif-Cormerais, M. Masana, J. Van de Weijer, and B. Twardowski, “On the importance of cross-task features for class-incremental learning,” *arXiv preprint arXiv:2106.11930*, vol. 1, 2021.
- [9] L. Wang, X. Zhang, H. Su, and J. Zhu, “A comprehensive survey of continual learning: theory, method and application,” *IEEE Transactions on Pattern Analysis and Machine Intelligence*, 2024.
- [10] P. Buzzega, M. Boschini, A. Porrello, D. Abati, and S. Calderara, “Dark experience for general continual learning: a strong, simple baseline,” *Advances in neural information processing systems*, vol. 33, pp. 15 920–15 930, 2020.
- [11] M. Masana, X. Liu, B. Twardowski, M. Menta, A. D. Bagdanov, and J. Van De Weijer, “Class-incremental learning: survey and performance evaluation on image classification,” *IEEE Transactions on Pattern Analysis and Machine Intelligence*, vol. 45, no. 5, pp. 5513–5533, 2022.
- [12] E. J. Hu, Y. Shen, P. Wallis, Z. Allen-Zhu, Y. Li, S. Wang, L. Wang, and W. Chen, “Lora: Low-rank adaptation of large language models,” *arXiv preprint arXiv:2106.09685*, 2021.
- [13] S. Chen, C. Ge, Z. Tong, J. Wang, Y. Song, J. Wang, and P. Luo, “Adaptformer: Adapting vision transformers for scalable visual recognition,” *Advances in Neural Information Processing Systems*, vol. 35, pp. 16 664–16 678, 2022.
- [14] B. Lester, R. Al-Rfou, and N. Constant, “The power of scale for parameter-efficient prompt tuning,” in *Proceedings of the 2021 Conference on Empirical Methods in Natural Language Processing*, M.-F. Moens, X. Huang, L. Specia, and S. W.-t. Yih, Eds. Online and Punta Cana, Dominican Republic: Association for Computational Linguistics, Nov. 2021, pp. 3045–3059. [Online]. Available: <https://aclanthology.org/2021.emnlp-main.243>
- [15] D. Lian, D. Zhou, J. Feng, and X. Wang, “Scaling & shifting your features: A new baseline for efficient model tuning,” *Advances in Neural Information Processing Systems*, vol. 35, pp. 109–123, 2022.
- [16] Z. Wang, Z. Zhang, C.-Y. Lee, H. Zhang, R. Sun, X. Ren, G. Su, V. Perot, J. Dy, and T. Pfister, “Learning to prompt for continual learning,” in *Proceedings of the IEEE/CVF conference on computer vision and pattern recognition*, 2022, pp. 139–149.
- [17] Y.-S. Liang and W.-J. Li, “Inflora: Interference-free low-rank adaptation for continual learning,” in *Proceedings of the IEEE/CVF Conference on Computer Vision and Pattern Recognition*, 2024, pp. 23 638–23 647.
- [18] X. Gao, S. Dong, Y. He, Q. Wang, and Y. Gong, “Beyond prompt learning: Continual adapter for efficient rehearsal-free continual learning,” *arXiv preprint arXiv:2407.10281*, 2024.
- [19] Z. Wang, Z. Zhang, S. Ebrahimi, R. Sun, H. Zhang, C.-Y. Lee, X. Ren, G. Su, V. Perot, J. Dy *et al.*, “Dualprompt: Complementary prompting for rehearsal-free continual learning,” in *European Conference on Computer Vision*. Springer, 2022, pp. 631–648.
- [20] J. S. Smith, L. Karlinsky, V. Gutta, P. Cascante-Bonilla, D. Kim, A. Arbelle, R. Panda, R. Feris, and Z. Kira, “Coda-prompt: Continual decomposed attention-based prompting for rehearsal-free continual learning,” in *Proceedings of the IEEE/CVF Conference on Computer Vision and Pattern Recognition*, 2023, pp. 11 909–11 919.
- [21] D.-W. Zhou, H.-L. Sun, H.-J. Ye, and D.-C. Zhan, “Expandable subspace ensemble for pre-trained model-based class-incremental learning,” in *Proceedings of the IEEE/CVF Conference on Computer Vision and Pattern Recognition*, 2024, pp. 23 554–23 564.
- [22] K. Wei, X. Yang, Z. Xu, and C. Deng, “Class-incremental unsupervised domain adaptation via pseudo-label distillation,” *IEEE Transactions on Image Processing*, vol. 33, pp. 1188–1198, 2024.
- [23] L. Bonicelli, M. Boschini, A. Porrello, C. Spampinato, and S. Calderara, “On the effectiveness of lipschitz-driven rehearsal in continual learning,” *Advances in Neural Information Processing Systems*, vol. 35, pp. 31 886–31 901, 2022.
- [24] R. Aljundi, E. Belilovsky, T. Tuytelaars, L. Charlin, M. Caccia, M. Lin, and L. Page-Caccia, “Online continual learning with maximal interfered retrieval,” *Advances in neural information processing systems*, vol. 32, 2019.
- [25] R. Aljundi, M. Lin, B. Goujaud, and Y. Bengio, “Gradient based sample

- selection for online continual learning,” *Advances in neural information processing systems*, vol. 32, 2019.
- [26] Y. Zhou, J. Yao, F. Hong, Y. Zhang, and Y. Wang, “Balanced destruction-reconstruction dynamics for memory-replay class incremental learning,” *IEEE Transactions on Image Processing*, 2024.
- [27] S. Jung, H. Ahn, S. Cha, and T. Moon, “Continual learning with node-importance based adaptive group sparse regularization,” *Advances in neural information processing systems*, vol. 33, pp. 3647–3658, 2020.
- [28] F. Zenke, B. Poole, and S. Ganguli, “Continual learning through synaptic intelligence,” in *International conference on machine learning*. PMLR, 2017, pp. 3987–3995.
- [29] J. Lu and S. Sun, “Pamk: Prototype augmented multi-teacher knowledge transfer network for continual zero-shot learning,” *IEEE Transactions on Image Processing*, 2024.
- [30] B. Qiu, H. Qiu, H. Wen, L. Wang, Y. Dai, F. Meng, Q. Wu, and H. Li, “Geodesic-aligned gradient projection for continual task learning,” *IEEE Transactions on Image Processing*, 2025.
- [31] C.-Y. Hung, C.-H. Tu, C.-E. Wu, C.-H. Chen, Y.-M. Chan, and C.-S. Chen, “Compacting, picking and growing for forgetting continual learning,” *Advances in neural information processing systems*, vol. 32, 2019.
- [32] X. Li, Y. Zhou, T. Wu, R. Socher, and C. Xiong, “Learn to grow: A continual structure learning framework for overcoming catastrophic forgetting,” in *International conference on machine learning*. PMLR, 2019, pp. 3925–3934.
- [33] S. Yan, J. Xie, and X. He, “Der: Dynamically expandable representation for class incremental learning,” in *Proceedings of the IEEE/CVF conference on computer vision and pattern recognition*, 2021, pp. 3014–3023.
- [34] X. Wang, Z. Ji, Y. Yu, Y. Pang, and J. Han, “Model attention expansion for few-shot class-incremental learning,” *IEEE Transactions on Image Processing*, 2024.
- [35] B. Ermiş, G. Zappella, M. Wistuba, A. Rawal, and C. Archambeau, “Memory efficient continual learning with transformers,” *Advances in Neural Information Processing Systems*, vol. 35, pp. 10629–10642, 2022.
- [36] H. Wang, D. Cheng, L. He, Y. Li, J. Li, N. Wang, and X. Gao, “Ekpc: Elastic knowledge preservation and compensation for class-incremental learning,” *arXiv preprint arXiv:2506.12351*, 2025.
- [37] H. Wang, D. Cheng, G. Li, Z. Xu, L. He, J. Li, N. Wang, and X. Gao, “Stpr: Spatiotemporal preservation and routing for exemplar-free video class-incremental learning,” *arXiv preprint arXiv:2505.13997*, 2025.
- [38] D. Cheng, Y. Lu, L. He, S. Zhang, X. Yang, N. Wang, and X. Gao, “Mamba-cl: Optimizing selective state space model in null space for continual learning,” *arXiv preprint arXiv:2411.15469*, 2024.
- [39] M. Boschini, L. Bonicelli, A. Porrello, G. Bellitto, M. Pennisi, S. Palazzo, C. Spampinato, and S. Calderara, “Transfer without forgetting,” in *European Conference on Computer Vision*. Springer, 2022, pp. 692–709.
- [40] G. Zhang, L. Wang, G. Kang, L. Chen, and Y. Wei, “Slca: Slow learner with classifier alignment for continual learning on a pre-trained model,” in *Proceedings of the IEEE/CVF International Conference on Computer Vision*, 2023, pp. 19 148–19 158.
- [41] Z. Gao, J. Cen, and X. Chang, “Consistent prompting for rehearsal-free continual learning,” in *Proceedings of the IEEE/CVF Conference on Computer Vision and Pattern Recognition*, 2024, pp. 28 463–28 473.
- [42] J. Qiao, X. Tan, C. Chen, Y. Qu, Y. Peng, Y. Xie *et al.*, “Prompt gradient projection for continual learning,” in *The Twelfth International Conference on Learning Representations*, 2023.
- [43] N. Houlsby, A. Giurgiu, S. Jastrzebski, B. Morrone, Q. De Laroussilhe, A. Gesmundo, M. Attariyan, and S. Gelly, “Parameter-efficient transfer learning for nlp,” in *International conference on machine learning*. PMLR, 2019, pp. 2790–2799.
- [44] X. L. Li and P. Liang, “Prefix-tuning: Optimizing continuous prompts for generation,” in *Proceedings of the 59th Annual Meeting of the Association for Computational Linguistics and the 11th International Joint Conference on Natural Language Processing (Volume 1: Long Papers)*, C. Zong, F. Xia, W. Li, and R. Navigli, Eds. Online: Association for Computational Linguistics, Aug. 2021, pp. 4582–4597. [Online]. Available: <https://aclanthology.org/2021.acl-long.353>
- [45] M. Jia, L. Tang, B.-C. Chen, C. Cardie, S. Belongie, B. Hariharan, and S.-N. Lim, “Visual prompt tuning,” in *European Conference on Computer Vision*. Springer, 2022, pp. 709–727.
- [46] D. Cheng, Z. Xu, X. Jiang, N. Wang, D. Li, and X. Gao, “Disentangled prompt representation for domain generalization,” in *Proceedings of the IEEE/CVF Conference on Computer Vision and Pattern Recognition*, 2024, pp. 23 595–23 604.
- [47] Z. Xu, D. Cheng, X. Jiang, N. Wang, D. Li, and X. Gao, “Adversarial domain prompt tuning and generation for single domain generalization,” in *Proceedings of the Computer Vision and Pattern Recognition Conference*, 2025, pp. 18 584–18 595.
- [48] C. Zhao, Y. Wang, X. Jiang, Y. Shen, K. Song, D. Li, and D. Miao, “Learning domain invariant prompt for vision-language models,” *IEEE Transactions on Image Processing*, vol. 33, pp. 1348–1360, 2024.
- [49] S. Xuan, M. Yang, and S. Zhang, “Adapting vision-language models via learning to inject knowledge,” *IEEE Transactions on Image Processing*, 2024.
- [50] R. A. Jacobs, M. I. Jordan, S. J. Nowlan, and G. E. Hinton, “Adaptive mixtures of local experts,” *Neural computation*, vol. 3, no. 1, pp. 79–87, 1991.
- [51] A. Dosovitskiy, “An image is worth 16x16 words: Transformers for image recognition at scale,” *arXiv preprint arXiv:2010.11929*, 2020.
- [52] S. Wang, X. Li, J. Sun, and Z. Xu, “Training networks in null space of feature covariance for continual learning,” in *Proceedings of the IEEE/CVF conference on Computer Vision and Pattern Recognition*, 2021, pp. 184–193.
- [53] Q. Gao, C. Zhao, Y. Sun, T. Xi, G. Zhang, B. Ghanem, and J. Zhang, “A unified continual learning framework with general parameter-efficient tuning,” in *Proceedings of the IEEE/CVF International Conference on Computer Vision*, 2023, pp. 11 483–11 493.
- [54] D.-W. Zhou, Z.-W. Cai, H.-J. Ye, D.-C. Zhan, and Z. Liu, “Revisiting class-incremental learning with pre-trained models: Generalizability and adaptivity are all you need,” *International Journal of Computer Vision*, pp. 1–21, 2024.
- [55] L. Huang, X. Cao, H. Lu, and X. Liu, “Class-incremental learning with clip: Adaptive representation adjustment and parameter fusion,” 2024. [Online]. Available: <https://arxiv.org/abs/2407.14143>
- [56] L. Jiao, Q. Lai, Y. Li, and Q. Xu, “Vector quantization prompting for continual learning,” *arXiv preprint arXiv:2410.20444*, 2024.
- [57] J. Li, S. Wang, B. Qian, Y. He, X. Wei, Q. Wang, and Y. Gong, “Dynamic integration of task-specific adapters for class incremental learning,” in *Proceedings of the Computer Vision and Pattern Recognition Conference*, 2025, pp. 30 545–30 555.
- [58] T. Fukuda, H. Kera, and K. Kawamoto, “Adapter merging with centroid prototype mapping for scalable class-incremental learning,” in *Proceedings of the Computer Vision and Pattern Recognition Conference*, 2025, pp. 4884–4893.
- [59] H. Wang, H. Lu, L. Yao, and D. Gong, “Self-expansion of pre-trained models with mixture of adapters for continual learning,” in *Proceedings of the Computer Vision and Pattern Recognition Conference*, 2025, pp. 10 087–10 098.
- [60] X. Liu and X. Chang, “Lora subtraction for drift-resistant space in exemplar-free continual learning,” in *Proceedings of the Computer Vision and Pattern Recognition Conference*, 2025, pp. 15 308–15 318.
- [61] J. He, Z. Duan, and F. Zhu, “Cl-lora: Continual low-rank adaptation for rehearsal-free class-incremental learning,” in *Proceedings of the Computer Vision and Pattern Recognition Conference*, 2025, pp. 30 534–30 544.
- [62] W.-C. Huang, C.-F. Chen, and H. Hsu, “OVOR: Oneprompt with virtual outlier regularization for rehearsal-free class-incremental learning,” in *The Twelfth International Conference on Learning Representations*, 2024. [Online]. Available: <https://openreview.net/forum?id=FbuyDzZTPt>
- [63] A. Roy, R. Moullick, V. K. Verma, S. Ghosh, and A. Das, “Convolutional prompting meets language models for continual learning,” in *Proceedings of the IEEE/CVF Conference on Computer Vision and Pattern Recognition*, 2024, pp. 23 616–23 626.
- [64] D. Hendrycks, S. Basart, N. Mu, S. Kadavath, F. Wang, E. Dorundo, R. Desai, T. Zhu, S. Parajuli, M. Guo *et al.*, “The many faces of robustness: A critical analysis of out-of-distribution generalization,” in *Proceedings of the IEEE/CVF international conference on computer vision*, 2021, pp. 8340–8349.
- [65] D. Hendrycks, K. Zhao, S. Basart, J. Steinhardt, and D. Song, “Natural adversarial examples,” in *Proceedings of the IEEE/CVF conference on computer vision and pattern recognition*, 2021, pp. 15 262–15 271.
- [66] A. Krizhevsky, G. Hinton *et al.*, “Learning multiple layers of features from tiny images,” 2009.
- [67] X. Peng, Q. Bai, X. Xia, Z. Huang, K. Saenko, and B. Wang, “Moment matching for multi-source domain adaptation,” in *Proceedings of the IEEE/CVF international conference on computer vision*, 2019, pp. 1406–1415.
- [68] O. Russakovsky, J. Deng, H. Su, J. Krause, S. Satheesh, S. Ma, Z. Huang, A. Karpathy, A. Khosla, M. Bernstein *et al.*, “Imagenet large

scale visual recognition challenge,” *International journal of computer vision*, vol. 115, pp. 211–252, 2015.

- [69] Y. Wang, Z. Ma, Z. Huang, Y. Wang, Z. Su, and X. Hong, “Isolation and impartial aggregation: A paradigm of incremental learning without interference,” in *Proceedings of the AAAI Conference on Artificial Intelligence*, vol. 37, no. 8, 2023, pp. 10 209–10 217.
- [70] I. E. Marouf, S. Roy, E. Tartaglione, and S. Lathuilière, “Weighted ensemble models are strong continual learners,” *arXiv preprint arXiv:2312.08977*, 2023.
- [71] C. Wah, S. Branson, P. Welinder, P. Perona, and S. Belongie, “The caltech-ucsd birds-200-2011 dataset,” 2011.
- [72] J. Krause, M. Stark, J. Deng, and L. Fei-Fei, “3d object representations for fine-grained categorization,” in *Proceedings of the IEEE international conference on computer vision workshops*, 2013, pp. 554–561.
- [73] D. Jung, D. Han, J. Bang, and H. Song, “Generating instance-level prompts for rehearsal-free continual learning,” in *Proceedings of the IEEE/CVF International Conference on Computer Vision*, 2023, pp. 11 847–11 857.
- [74] J. S. Smith, Y.-C. Hsu, L. Zhang, T. Hua, Z. Kira, Y. Shen, and H. Jin, “Continual diffusion: Continual customization of text-to-image diffusion with c-lora,” *arXiv preprint arXiv:2304.06027*, 2023.
- [75] L. Wang, J. Xie, X. Zhang, M. Huang, H. Su, and J. Zhu, “Hierarchical decomposition of prompt-based continual learning: Rethinking obscured sub-optimality,” *Advances in Neural Information Processing Systems*, vol. 36, 2024.
- [76] M. Caron, H. Touvron, I. Misra, H. Jégou, J. Mairal, P. Bojanowski, and A. Joulin, “Emerging properties in self-supervised vision transformers,” in *Proceedings of the IEEE/CVF international conference on computer vision*, 2021, pp. 9650–9660.
- [77] J. Zhou, C. Wei, H. Wang, W. Shen, C. Xie, A. Yuille, and T. Kong, “ibot: Image bert pre-training with online tokenizer,” *arXiv preprint arXiv:2111.07832*, 2021.



Lingfeng He received the B.Sc. degree from Xidian University, Xi’an, China, in 2023. He is currently pursuing his M.S. degree in Information and Communication Engineering in Xidian University. His research interests include person re-identification, unsupervised learning and continual learning.



De Cheng received the B.S. and Ph.D. degrees from Xi’an Jiaotong University, Xi’an, China, in 2011 and 2017, respectively. He is currently an Associate Professor with the School of Telecommunications Engineering, Xidian University, Xi’an. From 2015 to 2017, he was a Visiting Scholar with Carnegie Mellon University, Pittsburgh, PA, USA. His research interests include pattern recognition, machine learning, and multimedia analysis.



Zhiheng Ma received the PhD degree from Xi’an Jiaotong University, in 2021. He is a research assistant professor with the Shenzhen Institute of Advanced Technology, Chinese Academy of Sciences (SIAT). He has authored articles in journals and conferences, such as IEEE Transactions on Image Processing, CVPR, ICCV, and AAAI. His current research interests include incremental learning, crowd counting, and novelty detection.



Huaijie Wang received the B.Sc. degree from Xidian University, Xi’an, China, in 2024. He is currently pursuing his Ph.D. degree in School of Electronic Engineering in Xidian University. His research interest is continual learning.



Dingwen Zhang is a professor with School of Automation, Northwestern Polytechnical University, Xi’an, China. He received his Ph.D. degree from NPU in 2018. From 2015 to 2017, he was a visiting scholar at the Robotic Institute, Carnegie Mellon University, Pittsburgh, United States. His research interests include computer vision and multimedia processing, especially on saliency detection and weakly supervised learning.



Nannan Wang received the B.S. degree in information and computation science from the Xi’an University of Posts and Telecommunications in 2009 and the Ph.D. degree in information and telecommunications engineering from Xidian University in 2015. From September 2011 to September 2013, he was a Visiting Ph.D. Student with the University of Technology Sydney, Australia. He is currently a Professor with the State Key Laboratory of Integrated Services Networks, Xidian University.



Xinbo Gao (M’02-SM’07) received the B.Eng., M.Sc. and Ph.D. degrees in electronic engineering, signal and information processing from Xidian University, Xi’an, China, in 1994, 1997, and 1999, respectively. From 1997 to 1998, he was a Research Fellow with the Department of Computer Science, Shizuoka University, Shizuoka, Japan. From 2000 to 2001, he was a Post-Doctoral Research Fellow with the Department of Information Engineering, the Chinese University of Hong Kong, Hong Kong. Since 2001, he has been with the School of Electronic Engineering, Xidian University. He is also a Cheung Kong Professor of the Ministry of Education of China, a Professor of Pattern Recognition and Intelligent System with Xidian University, and a Professor of Computer Science and Technology with the Chongqing University of Posts and Telecommunications, Chongqing, China. He has published 6 books and around 300 technical articles in refereed journals and proceedings. His research interests include image processing, computer vision, multimedia analysis, machine learning, and pattern recognition. Prof. Gao is also a Fellow of the Institute of Engineering and Technology and the Chinese Institute of Electronics. He has served as the general chair/cochair, the program committee chair/co-chair, or a PC member for around 30 major international conferences. He is also on the Editorial Boards of several journals, including Signal Processing (Elsevier) and Neurocomputing (Elsevier).